www.elsevier.com/locate/jmbbm

The anisotropic mechanical behaviour of electro-spun biodegradable polymer scaffolds. Experimental characterisation and constitutive formulation

Georges Limbert, Rodaina Omar, Hugo Krynauw, Deon Bezuidenhout, Thomas Franz

PII: S1751-6161(15)00255-6
DOI: http://dx.doi.org/10.1016/j.jmbbm.2015.07.014
Reference: JMBBM1544

To appear in: *Journal of the Mechanical Behavior of Biomedical Materials*

Received date: 20 January 2015
Revised date: 7 July 2015
Accepted date:
16 July 2015

Cite this article as: Georges Limbert, Rodaina Omar, Hugo Krynauw, Deon Bezuidenhout, Thomas Franz, The anisotropic mechanical behaviour of electro-spun biodegradable polymer scaffolds. Experimental characterisation and constitutive formulation, *Journal of the Mechanical Behavior of Biomedical Materials*, http://dx.doi.org/10.1016/j.jmbbm.2015.07.014

The anisotropic mechanical behaviour of electro-spun biodegradable polymer scaffolds. Experimental characterisation and constitutive formulation.

Georges Limbert[a, b, c*], Rodaina Omar[d], Hugo Krynauw[d], Deon Bezuidenhout[d], Thomas Franz[c, e, f]

[a] national Centre for Advanced Tribology at Southampton (nCATS), Engineering Sciences, Faculty of Engineering and the Environment, University of Southampton, Southampton SO17 1BJ, UK
[b] Bioengineering Science Research Group, Engineering Sciences, Faculty of Engineering and the Environment, University of Southampton, Southampton SO17 1BJ, UK
[c] Division of Biomedical Engineering, Department of Human Biology, Faculty of Health Sciences, University of Cape Town, Observatory 7935, South Africa
[d] Cardiovascular Research Unit, Chris Barnard Department of Cardiothoracic Surgery, Faculty of Health Sciences, University of Cape Town, Observatory 7935, South Africa
[e] Centre for Research in Computational and Applied Mechanics, University of Cape Town, Rondebosch 7701, South Africa
[f] Research Office, University of Cape Town, Mowbray 7701, South Africa

Abstract

Electro-spun biodegradable polymer fibrous structures exhibit anisotropic mechanical properties dependent on the degree of fibre alignment. Degradation and mechanical anisotropy need to be captured in a constitutive formulation when computational modelling is used in the development and design optimisation of such scaffolds.

Biodegradable polyester-urethane scaffolds were electro-spun and underwent uniaxial tensile testing in and transverse to the direction of predominant fibre alignment before and after in vitro degradation of up to 28 days. A microstructurally-based transversely isotropic hyperelastic continuum constitutive formulation was developed and its parameters were identified from the experimental stress-strain data of the scaffolds at various stages of degradation.

During scaffold degradation, maximum stress and strain in circumferential direction decreased from 1.02±0.23 MPa to 0.38±0.004 MPa and from 46±11% to 12±2%, respectively. In longitudinal direction, maximum stress and strain decreased from 0.071±0.016 MPa to 0.010±0.007 MPa and from 69±24% to 8±2%, respectively. The constitutive parameters were identified for both directions of the non-degraded and degraded scaffold for strain range varying between 0% and 16% with coefficients of determination $r^2 > 0.871$. The six-parameter constitutive formulation proved versatile enough to capture the varying non-linear transversely isotropic behaviour of the fibrous scaffold throughout various stages of degradation.

Key words

Polymer, biodegradable, electro-spinning, mechanical properties, transverse isotropy, constitutive modelling

Journal:	Journal of the Mechanical Behavior of Biomedical Materials
Article type:	Research Article
Date:	4 July 2015 (Revision 1)
***Corresponding author:**	Tel: +44 (0)2380 592381; fax: +44 (0)2380 593016. E-mail address: g.limbert@soton.ac.uk

1. Introduction

Regenerative medicine has emerged as one of the most dynamic drivers in the development of advanced engineered biomaterial solutions for tissue engineering applications (Furth et al., 2007; Williams, 2006). One crucial element in regenerative medicine are scaffolds that facilitate and guide the engineering and regeneration of biological tissues according to the application.

Scaffolds need to be designed so as to promote engineering and regenerating tissue such that the newly created tissue biologically and mechanically mimics the healthy host tissue (Furth et al., 2007). In the treatment of cardiovascular diseases, applications for regenerative medicine include tissue regenerative small-diameter vascular grafts which remain one of the major challenges to date (Zilla et al., 2007). In such grafts, porosity is a key factor for the long term success (Zilla et al., 2007). One method of introducing porosity in scaffolds for the engineering of soft biological tissues, such as vascular tissue, is electro-spinning of polymers (Braghirolli et al., 2014; Rocco et al., 2014). This technology results in fibrous polymeric networks. Process parameters allow controlling the degree of alignment of the fibres (Ayres et al., 2007; Wu et al., 2010) – a parameter that affects the mechanical properties of the scaffold. Scaffolds with fibres randomly distributed typically exhibit similar properties in different directions whereas the alignment of fibres predominantly in one direction introduces mechanical anisotropy (Ayres et al., 2007). Electro-spun scaffolds with a high degree of fibre alignment exhibit a higher elastic modulus, i.e. stiffness, in fibre direction and a lower elastic modulus perpendicular to the fibre direction. The directional mechanical properties of the scaffold can be utilised to tailor the structural properties of the engineered tissue. They add, however, complexity to the design process which needs to be adequately addressed.

Regeneration of biological tissues without any synthetic material remaining in the engineered construct can be facilitated with scaffolds materials that degrade *in vivo*. The degradation of the scaffold material introduces a transient process that affects the structural properties of the scaffold (Dargaville et al., 2013; Krynauw et al., 2011) and consequently engineering tissue (Roh et al., 2008). It is important to ensure that the degradation of the scaffold does not lead to premature failure of the tissue construct e.g. when the scaffold's disintegration rate is not adequately balanced with the rate of tissue ingrowth.

When computational modelling is utilised to assist in the development of tissue-regenerative scaffolds and tissue-engineered constructs, the numerical representation of the mechanical and structural properties of the scaffold, and the changes thereof described above, is imperative. It is therefore essential to have access to appropriate constitutive models (or constitutive laws) which, in a purely mechanical context, are sets of mathematical equations relating stress to strain. These mathematical relations can then be implemented in a computational environment, typically a finite element application, to subsequently carry out mechanical simulations on tissue engineering constructs for various loading scenarios and operating conditions.
To computationally model the mechanical response of a polymer-based fibrous scaffold one could take a *microstructural* or *phenomenological* approach. In the former approach, the geometry of the electro-spun fibres would be explicitly modelled and assigned isotropic properties of the bulk polymer material. In that case, mechanical anisotropy of the scaffold would arise as a consequence of its structural properties. The second modelling approach would consider the fibrous scaffold as a single bulk structure made of a homogeneous material, therefore disregarding the explicit geometry of polymer fibres. A constitutive model capturing the physical transversely isotropic behaviour of electro-spun fibre scaffold would then be assigned to the scaffold which would effectively be modelled as a macroscopic structure governed by a macroscopic phenomenological constitutive law. In this work, the latter approach is pursued and is described in **section 3**.

Biodegradable polymers used for medical device, tissue engineering and regenerative medicine applications typically operate in complex conditions whether it is from the viewpoint of the biochemical or mechanical environment (Riboldi et al., 2005; Soares et al., 2010b). Structures made of biodegradable polymers generally are subjected to strain rate-sensitive cyclic loads sufficient to induce large elastic and/or inelastic strains operating in the non-linear regime (Grabow et al., 2013; Vieira et al., 2014; Vieira et al., 2013). It is therefore important to consider constitutive models that, depending on particular applications, can capture specific features such as large deformations. For example, in that case, this consideration rules out Hooke's elasticity as a suitable constitutive model. Of course, a key feature of biodegradable polymers is their inherent propensity to have their mechanical strength reduced as a result of chemo-mechanical damage. Several constitutive models accounting for these phenomena have been proposed.

Notably, Soares et al. (2007; 2010c; Soares and Zunino, 2010b) developed 3D constitutive models based on hyperelastic potentials combined with damage laws to represent deformation-induced hydrolysis (Soares et al., 2010c). They also proposed a mathematical mixture model capturing water-dependent degradation and erosion as well as drug release (Soares and Zunino, 2010a).
In the study by Vieira et al. (2011), several hyperelastic strain energy functions were assessed to represent the purely mechanical behaviour of biodegradable aliphatic polyester fibres. The constitutive formulation was augmented to account for water diffusion, hydrolytic damage, surface and bulk erosion.

The time-dependent behaviour of biodegradable polymers has been demonstrated in many studies (Grabow et al., 2007; Soares, 2008) and references therein. Based on the concept of quasi-linear viscoelasticity Muliana and Rajagopal (2012a) proposed a viscoelastic constitutive model featuring deformation-dependent rate of degradation which was later extended with a degradation term arising from water diffusion (Muliana and Rajagopal, 2012b). Khan and El-Sayed (2013) derived a non-linear viscohyperelastic formulation based on conservative and dissipative potentials which also accounted for deformation-induced degradation following the work of Soares (2008). Recently, Vieira et al. (2014) proposed what probably is the most advanced 3D continuum constitutive model for biodegradable polymers with regards to the purely mechanical behaviour. The constitutive behaviour is based on the micromechanically-based strain rate-dependent Bergström-Boyce formulation for polymers (Bergstrom and Boyce, 1998). Vieira et al's model is equipped with damage equations inspired from polymer chain scission kinetics to model hydrolysis-induced degradation. Chen and Li (2010) and Chen et al. (2011) proposed mathematical models of biodegradable polymers featuring stochastic hydrolysis, degradation and erosion through mass transport equations.

Some of the constitutive models described above are able to capture the isotropic, large deformation, rate-dependent, cyclic inelastic behaviour of biodegradable polymers combined with mechanical and/or chemo-mechanical degradation. However, none of these constitutive models capture any anisotropic behaviour such as that that would be required to provide a phenomenological description of electro-spun fibres network made of such a material.

Most of the continuum constitutive models for electro-spun polymer fibre network found in the literature take a microstructural stance by modelling the micromechanics of fibre networks and link it to the macroscopic behaviour of the mesh structure. For example, recently, D'Amore et al. (2014) developed an experimentally-supported microstructural finite element framework to represent the isotropic and anisotropic behaviour of electro-spun polyurethane and polyethylene terephthalate scaffolds. Using a combination of atomic force microscopy to measure fibre stress-strain characteristics and image processing to capture the statistics of fibre/mesh geometry, the modelling part consists in generating a synthetic fibre network made of beam finite elements emulating the real fibrous architecture and conduct subsequent finite element analyses replicating macroscopic-level biaxial traction tests. With a single material model, the authors successfully reproduced the five experiments considered. Courtney et al. (2006) proposed a structural fibre-level constitutive model for electro-spun poly (ester urethane) ureas used for tissue engineering scaffold applications. The formulation is able to capture particular statistical distributions of fibre orientation—isotropic or anisotropic and also accounts for the degree of crimping of the polymeric fibres. The model was fitted to planar equi-biaxial tensile test data corresponding to scaffolds produced at different electro-spinning velocities. As in Stella et al. (2010) it was observed that fibre alignment increased with mandrel velocity.

Constitutive and statistical models of non-woven microscopic fibrous structures have been developed to answer fundamental questions about the nature of scale-bridging mechanisms mediated by fibres, the relationships between geometrical fibre network characteristics (e.g. fibre diameter, orientation, packing density), stiffness of fibres and macroscopic mechanical response under a variety of loading conditions (Chandran and Barocas, 2006; Hatami-Marbini and Picu, 2009; Pence et al., 2008; Rizvi and Pal, 2014; Sander et al., 2009; Sastry et al., 1998; Sastry et al., 2001; Silberstein et al., 2012; Stylianopoulos et al., 2008; Wang et al., 2000; Wang and Sastry, 2000; Wu and Dzenis, 2005). These models, often based on multiscale approaches using volume-averaging theories (Stylianopoulos et al., 2008) are typically restricted to two-dimensional arrangements and/or do not easily generalise to three-dimensional continua. Although very insightful, in a finite element context, these approaches are not the most appropriate to simulate the macroscopic behaviour of whole structures made of fibrous network such as those generated by electro-spinning processes because of the high computational cost in simulating their behaviour.

It is therefore advantageous to have access to simple 3D constitutive laws that can capture the characteristic transversely isotropic behaviour of highly aligned electro-spun polymeric scaffolds like those produced for applications in cardiovascular tissue regeneration.

To address this need, it is proposed here to formulate a constitutive law capturing the transversely isotropic hyperelastic response of biodegradable electro-spun polymer fibre scaffold for moderate range of deformations (i.e. prior to initiation of failure) and for *in vitro* degradation times. The present focus is on the anisotropic response at specific fixed degradation times and not on the inelastic deformations and degradation processes that will be the object of a subsequent work. Again, it is emphasised that we depart from discrete approaches considering the mechanics of fibrous network using statistical descriptions or explicit fibre geometry and rather consider a 3D microstructurally-motivated continuum constitutive formulation.

To inform and validate the formulation of the phenomenological constitutive model biodegradable polyester-urethane scaffolds were electro-spun and underwent orthogonal uniaxial tensile testing in and transverse to the direction of predominant fibre alignment before and after *in vitro* degradation of up to 28 days (**section 2**). In **section 3** of the manuscript, a transverse-isotropic constitutive formulation is developed and material parameters are identified that best represent the experimental stress-strain data of the scaffolds at the various stages of degradation.

2. Materials and Methods

2.1 Scaffold and manufacturing and sample preparation

DegraPol® DP30 (ab medica S.p.A, Lainate, Italy), a biodegradable polyester-urethane comprising poly[*3-(R-hydroxybutyrate)-co-(ε-caprolactone)*]-*diol* and poly[ε caprolactone co glycolide]-diol (Milleret et al., 2009), linked with 2,2,4-trimethylhexamethylene diisocyanate (TMDI), was used in this study. Flat bulk samples were cast from solution of DegraPol® (24% by weight concentration) in chloroform by allowing complete evaporation of the solvent. For electro-spinning of fibrous scaffold structure, the DegraPol® solution was provided with a flow rate of 8 ml/h (SE400B syringe pump, Fresenius, Bad Homburg, Germany) through a hypodermic needle onto a rotating and bi-directionally translating tubular target (hypodermic tube, outer diameter: 25.4 mm, Small Parts, Loganport, IN, USA; rotational speed: 7200 RPM, translational speed: 2.6 mm/min, needle-target distance: 300 mm). An electrostatic potential of 15 kV between the feeder needle (15 kV) and the target (0 V) facilitated the spinning process. After completion of the spinning, tubular samples were submersed in ethanol for 5 minutes, cut open lengthwise, removed from the target tube and vacuum dried at room temperature for 90 min.

Rectangular samples were cut from the cast bulk DegraPol® material (7 x 22 mm), and from the tubular fibrous scaffold with the longer edges aligned with circumferential direction for circumferential samples and with the longitudinal direction of the tubular scaffold for longitudinal samples (10 x 20 mm). Sample dimensions were measured with a calliper except for wall thickness and width of fibrous samples which were measured on ×4 images (Leica DFC280 microscope, Leica Microsystems GmbH, Wetzlar, Germany).

2.2 *In vitro* scaffold degradation

Samples underwent *in vitro* hydrolytic degradation in phosphate buffered saline (PBS) in separate test tubes at 37 °C incubator shaking at 97 rpm. The PBS solution was changed at weekly intervals. Non-degraded samples were used as a reference of T = 0 day time point for all samples. For the investigation of the change in mechanical properties associated with degradation, samples were kept in the incubator for degradation periods of T = 4, 7, 11, 14, 17, 21, 24 and 28 days and tested as removed from the PBS.

For morphological characterisation, assessment of reduction in mass and molecular weight, samples (T= 7, 14, 21, and 28 days) were removed from PBS, rinsed thoroughly with distilled water to remove the residual PBS salts and dried overnight in a vacuum oven (Townson & Mercer, Stretford, England) at room temperature to stop and prevent degradation prior to assessments.

2.3 Scaffold characterisation

The fibre diameter was measured on ×2000 scanning electron micrographs (JSM5200, JEOL Ltd, Tokyo, Japan). The degree of fibre alignment in the electro-spun scaffold was determined by two-dimensional Fast Fourier Transforms (2D FFT) of ×100 SEM micrographs in ImageJ (National Institute of Health, Bethesda, MD, USA) using the Oval Profile Plot plug-in (written by William O'Connell) (Ayres et al., 2006; Ayres et al., 2007; Ayres et al., 2008).

The porosity π of the fibrous network was calculated from total volume v_T and fibre volume v_F of the scaffold as $\pi = 1 - v_F/v_T$. The total volume comprising fibres and inter-fibre spaces was calculated from wall thickness, width and length of the samples (n = 3). The fibre volume, i.e. volume occupied by fibres excluding inter-fibre spaces, was obtained from hydrostatic weighing. The dry sample was weighed twice: in air and thereafter following the elimination of air from the inter-fibre spaces by submersion in ethanol (Adam AAA250L analytical balance with Adam density determination kit, Adam Equipment Inc, Danbury, CT, USA).

The difference in mass of the scaffold sample measured in air, $m_S(air)$, and in ethanol, $m_S(ethanol)$, caused by the buoyancy force exerted on the submerged scaffold, equals the mass of the ethanol, $m_{ethanol}$, that is displaced by the fibres: $m_{ethanol} = m_s(air) - m_s(ethanol)$. The volume of the displaced ethanol, v_E, was calculated according to $v_E = m_{ethanol}/\rho_{ethanol}$ where $\rho_{ethanol}$ is the known density of ethanol. The volume of the ethanol displaced by the fibres equals the volume of the fibres, hence $v_F = v_E$.

Uniaxial tensile tests were performed on samples (n = 5) submerged in PBS at 37°C on an Instron 5544 universal testing machine with 10N load cell (Instron, Norwood, USA). The test protocol comprised a single extension until failure (strain rate: 9.6%/sec). The samples were tested in orthogonal directions (one test per sample) coinciding with circumferential and longitudinal directions of the tubular scaffold.
Key data reported include the maximum stress $\sigma_{\max}$and strain at first occurrence of maximum stress $\varepsilon_{\max}$. The elastic modulus E of all samples was measured as the slope of the linear equation that fits the stress-strain data recorded between 0 and 5% strain by using linear regression analysis of the data points.

Molecular weight changes during degradation were determined by gel permeation chromatography (GPC) (Roediger Agencies cc, Analytical Laboratories, Stellenbosch, South Africa). The system consisted of a Waters 510 HPLC pump, Waters 486 tuneable absorbance detector at 260 nm, Waters 410 differential refractometer and a Thermo Separations Products Spectra Series AS100 auto sampler. Five columns (Styragel®HR1 through HR6, Waters) and a pre-column filter were used at 30°C. Polystyrene standards were used for calibration. Samples were dissolved in THF (1mg/ml) at 37°C with sonication for 20min. Pump flow rate was set to 1.06 ml/min. The volume of the samples injected was 180 µl. DPSS Win GPC Scientific v4.02 was used for data analysis. Results are reported as weight average molecular weight (M_w).

3. Constitutive formulation

The constitutive formulation proposed here is based on the continuum theory of fibre reinforced composites (Spencer, 1992) where fibres are not explicitly modelled but rather accounted for through their micromechanical contribution via appropriate constitutive equations. This approach has been widely used in tissue biomechanics, particularly for biological soft tissues (Holzapfel et al., 2000; Humphrey and Yin, 1987; Kuhl et al., 2005; Limbert, 2011; Limbert and Taylor, 2002) which feature more or less complex arrangements of collagenous and non-structured proteins embedded in a soft matrix mainly composed of proteoglycans (Fung, 1981). An attractive feature of these types of formulation is that, although phenomenological in nature, they can incorporate microstructural deformation mechanisms.
To capture the mesh-like network characteristics of electro-spun scaffolds the 8-chain model approach first proposed by Arruda and Boyce (1993) in the context of polymer chain mechanics is followed but, borrowing from the elegant models of Bischoff et al. (2002a); (2002b) and Kuhl et al. (2005), modified by the introduction of two distinct characteristic dimensions of the micromechanical unit cell. However, departing from a classical entropic elasticity formulation for the stress-strain relation of polymer chains (Arruda and Boyce, 1993; Kratky and Porod, 1949), a novel formulation representing the mechanics of *polymeric fibres* (not polymer chains) is proposed.
The use of an eight-chain model is motivated by the desire to model the continuum mechanics and anisotropic characteristics of a structural material (subsequently referred as "electrospun scaffold material" or "scaffold material") using a simple formulation with a limited number of constitutive parameters. The original eight-chain model of Arruda and Boyce is known to provide good predictive capabilities in deformation modes other than those used for the identification of constitutive parameters.
It is assumed that, at the macroscopic scale, the scaffold material can be considered as a continuum composite assembly of polymer fibres oriented along a single preferred direction and non-fibrous polymer amorphous aggregates made of the bulk material DegraPol® DP30. This assumption is justified by the fact that the electro-spinning process generate polymer fibres which are not necessarily uniform in size and distribution, disjoint and that coalesce into non-homogeneous bulk aggregates (**Figure 5**-**Figure 6**). In reality, during macroscopic deformations, these polymer fibres mechanically interact mutually and with these non-fibrous aggregates. For modelling purpose, it can be assumed that the overall mechanical response of the scaffold material is made of two main contributions: one contribution of elastic polymer fibres acting in a network fashion (i.e. using a transversely isotropic eight-chain model) superimposed over a mechanical bulk contribution that represents the fibre kinetic interactions with bulk aggregates combined to the bulk response of these aggregates. It is worth reiterating that unlike the isotropic eight-chain model (Arruda and Boyce, 1993) which assumes a microscopic unit cell made of eight polymer *chain*s originating from each corner of the cell and mutually connected at the centre, the model proposed here considers polymer *fibres.* Therefore it can be viewed as a model operating at a higher spatial scale.

In summary, the constitutive model for the scaffold material is established through the definition of two fictitious strain energy functions. One strain energy function represents the dominant behaviour of electro-spun polymer fibres via a transversely isotropic eight-chain model (Kuhl et al., 2005) and the other captures the isotropic behaviour of amorphous polymer aggregates and models *implicitly* additional fibre-fibre and fibre-aggregate kinetic interactions. The elastic behaviour of polymer fibres will be defined by a dedicated strain energy density, first proposed by Knowles (1977).

Basic definitions of continuum mechanics entities necessary for the constitutive formulation are briefly reviewed. The deformation map φ which, at any given time t, maps the *material* placement $\mathbf{X}$ of a physical particle in the material configuration Ω_0 to its spatial counterpart, or *spatial* placement $\mathbf{x}$ in the *spatial* configuration is defined as $\mathbf{x} = \varphi(\mathbf{X}, t)$ (Marsden and Hughes, 1994). The deformation gradient with respect to the *material* coordinates is then defined as $\mathbf{F}(\mathbf{X}, t) = \partial\varphi(\mathbf{X}, t)/\,\partial\mathbf{X} = \nabla_{\mathbf{X}}\varphi(\mathbf{X}, t) = \partial\mathbf{x}/\,\partial\mathbf{X}$ and the Jacobian determinant of the deformation is $J = \det(\mathbf{F})$. Without loss of generality, it is assumed here that the kinematics of $\mathcal{B}$ is described using orthonormal bases in the Lagrangean and Eulerian configurations so that the two metric tensors reduce to the second-order identity tensor $\mathbf{I}$. The right and left Cauchy-Green deformation tensors are respectively defined as $\mathbf{C} = \mathbf{F}^{\mathrm{T}}\mathbf{F}$ and $\mathbf{b} = \mathbf{F}\mathbf{F}^{\mathrm{T}}$ where the superscript "T" denotes the transpose of a tensor. For subsequent developments, one also defines "$\otimes$" as the outer tensor product operator, ":" as the double contracted tensor product operator and $\det(\bullet)$ as the determinant of a tensor $\bullet$ (Holzapfel, 2000).

3.1 Material symmetry and invariant formulation

The simplest case of anisotropic material is represented by an isotropic solid matrix containing one family of fibres possessing a single preferred principal direction (at least, locally). This represents *transversely isotropic* symmetry. Any orthogonal transformation member of the symmetry group of the material must leave the strain energy function unchanged when applied to the material in the natural state (prior to deformation) (Ogden, 1984).
If $\mathbf{n}_0 = \mathbf{n}_0(\mathbf{X})$ represents the unit vector tangent to the local fibre orientation in the reference configuration, a set of five scalar-valued tensor invariants $\{I_i\}_{i=1..5}$ is necessary to form the *irreducible integrity bases* of the tensors $\mathbf{C}$ and $\mathbf{\Lambda}_0 = \mathbf{n}_0 \otimes \mathbf{n}_0$ (Boehler, 1978; Spencer, 1992). This means that there must exist a strain energy function $\Psi = \Psi(I_1, I_2, I_3, I_4, I_5)$ where the classical principal invariants of $\mathbf{C}$ are given by:

$$I_1 = \mathbf{C}\colon\mathbf{I}, \quad I_2 = \tfrac{1}{2}[I_1 - \mathbf{C}^2\colon\mathbf{I}], \quad I_3 = \det(\mathbf{C}) \tag{1}$$

and are augmented with anisotropic invariants I_4 and I_5 depending on $\mathbf{C}$ and the material structural tensor $\mathbf{\Lambda}_0$:

$$I_4 = \mathbf{C}\colon\mathbf{\Lambda}_0, \quad I_5 = \mathbf{C}^2\colon\mathbf{\Lambda}_0 \tag{2}$$

If λ denotes the stretch in the fibre direction n_0 defined by $\mathbf{F}\mathbf{n}_0 = \lambda\mathbf{n}$—$\mathbf{n}$ being the unit vector tangent to the fibre direction in the deformed configuration—it is straightforward to show that $\lambda^2 = I_4$ (Holzapfel, 2000).

3.2 Mechanical behaviour of individual polymer fibres

It is assumed that individual polymer fibres can be idealised as long regular solid cylinders of initial radius r_0 and length L_0 capable of sustaining tension only. It is further hypothesised that fibres obey a constitutive relationship first introduced by Knowles (1977) and used by Soares et al. (2010a) to model the continuum isotropic mechanical behaviour of biodegradable polymers:

$$\hat{\psi}_{chain} = \tfrac{c_1}{2c_2}\left[\left[1 + \tfrac{c_2}{p}(\hat{I}_1 - 3)\right]^p - 1\right];\ p > 0 \tag{3}$$

If one assumes that polymer chains are incompressible rods (Kuhl et al., 2005), the right Cauchy-Green deformation tensor $\hat{\mathbf{C}} = \hat{\mathbf{F}}^{\mathrm{T}}\hat{\mathbf{F}}$ characterising the elongation (associated with stretch $\hat{\lambda}$) of a single fibre along its main axis a_0 (direction of transverse isotropy, see **Figure 1**) is given by:

$$\hat{\mathbf{C}} = \hat{\lambda}^2\mathbf{a}_0 \otimes \mathbf{a}_0 + \tfrac{2}{\hat{\lambda}}(\mathbf{I} - \mathbf{a}_0 \otimes \mathbf{a}_0) \tag{4}$$

One can then define the first invariant of $\hat{\mathbf{C}}$ as:

$$\hat{I}_1 = \hat{\lambda}^2 + \tfrac{2}{\hat{\lambda}} \tag{5}$$

It follows that the Cauchy stress along the stretch direction a_0 is given by Moore et al. (2010):

$$\hat{\mathbf{S}}\mathbf{a}_0 = \frac{1}{J}\frac{\partial\hat{\psi}_{chain}}{\partial\hat{\mathbf{F}}}\hat{\mathbf{F}}^{\mathrm{T}}\mathbf{a}_0 = \hat{\mathrm{S}}\mathbf{a}_0\mathbf{a}_0 = \hat{\mathrm{S}} \tag{6}$$

$$\hat{\mathrm{S}} = c_1\left[1+\frac{c_2}{p}(\hat{\lambda}^2+\frac{2}{\hat{\lambda}}-3)\right]^{p-1}\left(\hat{\lambda}^2-\frac{1}{\hat{\lambda}}\right) \tag{7}$$

The current elongation force acting on an individual fibre of initial average radius r_0 is:

$$\hat{f}(\hat{\lambda}) = \frac{c_1\hat{\lambda}}{\pi r_0^2}\left[1+\frac{c_2}{p}(\hat{\lambda}^2+\frac{2}{\hat{\lambda}}-3)\right]^{p-1}\left(\hat{\lambda}^2-\frac{1}{\hat{\lambda}}\right) \tag{8}$$

The force-stretch relation can be normalised by the initial length of a fibre L_0:

$$f(\hat{\lambda}) = \frac{\hat{f}(\hat{\lambda})}{L_0} = \frac{c_1\hat{\lambda}}{\pi r_0^2 L_0}\left[1+\frac{c_2}{p}(\hat{\lambda}^2+\frac{2}{\hat{\lambda}}-3)\right]^{p-1}\left(\hat{\lambda}^2-\frac{1}{\hat{\lambda}}\right) \tag{9}$$

To describe the network properties of the biodegradable polymer fibres we consider a 8-chain representation which was developed by Arruda and Boyce (1993) for representing the mechanical network behaviour of rubber materials. This formulation was later extended to orthotropy (Bischoff et al., 2002a; Bischoff et al., 2002b, c) and transverse isotropy (Kuhl et al., 2005) in the context of biological soft tissues. Here, a transversely isotropic unit cell with initial cell dimensions ξ_a and ξ_b is considered (Kuhl et al., 2005) so that the directional reinforcement of the polymer structure is accounted for whilst also capturing the network characteristics of electro-spun fibres.

The ratio $\rho = \xi_a/\xi_b$ characterises the degree of anisotropy of the unit cell. When $\rho = 1$ isotropy is recovered. The eight chains are attached to the eight corners of the unit cell and link together at the centre of the cell (**Figure 2**). The strain energy of a single chain (in our case, a fibre or fibrous chain) is obtained by integrating the force-stretch relationship (9):

$$\psi_{chain} = \int f(u)du + \psi_{chain}^0 \tag{10}$$

The bulk properties of the biodegradable polymer are captured by a simple neo-Hookean-type strain energy function (Kuhl et al., 2005):

$$\psi_{bulk} = \frac{\mu}{2}\left[(I_1-3)+\frac{1}{\beta}(I_3^{-\beta}-1)\right] \tag{11}$$

where μ and β are constitutive parameters. As mentioned previously, it can be considered that this bulk energy function implicitly encompasses shear and volumetric stresses arising from the elasticity of amorphous polymer aggregates and their interactions with polymer fibres. Because there is an obvious intrinsic relationships between the scaffold apparent mechanical properties and those of the bulk polymeric material making up the electro-spun fibres, it is sensible to use identical constitutive parameters for the chain and bulk strain energies. This leads to $\mu/2 = c_1$. Only an additional parameter β is introduced to control the compressibility of the composite constitutive model. The bulk strain energy is therefore rewritten as:

$$\psi_{bulk} = c_1\left[(I_1-3)+\frac{1}{\beta}(I_3^{-\beta}-1)\right] \tag{12}$$

It is worth reiterating that Equation (3) applies to the bulk polymeric material while Equations (11)-(12) apply to the bulk "continuum scaffold material".

The length of a single polymer fibre (or "polymer chain" in the sense of the eight-chain model) in the *undeformed* configuration is:

$$l_0 = \frac{\sqrt{\xi_a^2+2\xi_b^2}}{2} \tag{13}$$

while the length of a *deformed* single polymer fibre is given by:

$$l = \frac{\sqrt{I_4\xi_a^2+(I_1-I_4)\xi_b^2}}{2} \tag{14}$$

The relative stretch of a polymer fibre λ_r is:

$$\lambda_r = \frac{l}{l_0} = \sqrt{\frac{I_4\xi_a^2 + (I_1 - I_4)\xi_b^2}{\xi_a^2 + 2\xi_b^2}} \tag{15}$$

One should point out that the invariants I_1, I_3 and I_4 are characteristic of the *macroscopic* deformations of the polymer. It is assumed that the microscopic stretch along the $\mathbf{a}_0$ direction is captured in an *affine* way through the macroscopic term I_4. This effectively couples the microscopic and macroscopic length scales giving rise to a multiscale model. The total strain energy of the polymer scaffold material is:

$$\psi(I_1, I_3, I_4) = (1 - \phi)\,\psi_{bulk}(I_1, I_3) + \phi\,\psi_{chain}(I_1, I_4) \tag{16}$$

where ϕ is the fibre volume fraction.

Assuming polymeric fibres can sustain tension only in the eight-chain conformation, the strain energy of a single fibre deformed to a length l is given by:

$$\psi_{chain} = \langle \lambda_r - 1 \rangle^0 \frac{c_1}{2c_2}\left[\left[1 + \frac{c_2}{p}\left(\lambda_r^2 + \frac{2}{\lambda_r} - 3\right)\right]^p - 1\right] \tag{17}$$

or, alternatively, using equation (15), as:

$$\psi_{chain} = \frac{c_1}{2c_2}\left\langle \sqrt{\frac{I_4\xi_a^2 + (I_1 - I_4)\xi_b^2}{\xi_a^2 + 2\xi_b^2}} - 1 \right\rangle^0 \left[\left[1 + \frac{c_2}{p}\left(\frac{I_4\xi_a^2 + (I_1 - I_4)\xi_b^2}{\xi_a^2 + 2\xi_b^2} + 2\sqrt{\frac{\xi_a^2 + 2\xi_b^2}{I_4\xi_a^2 + (I_1 - I_4)\xi_b^2}} - 3\right)\right]^p - 1\right] \tag{18}$$

where $\langle \bullet \rangle^0$ is the step function defined as:

$$\langle x - a \rangle^0 = \{1 \text{ if } x > a, 0 \text{ otherwise}\} = \frac{1}{2}\left(1 + \frac{x - a}{|x - a|}\right) \tag{19}$$

From the strain energy $\psi(I_1, I_3, I_4)$ one can derive the expression of the stress in the material as a function of the deformation/strain. The second Piola-Kirchhoff stress tensor is obtained by differentiation of equation (16) with respect to the right Cauchy-Green deformation tensor $\mathbf{C}$:

$$\mathbf{S} = 2\frac{\partial \Psi}{\partial \mathbf{C}} = 2\left((1 - \phi)\,\frac{\partial \psi_{bulk}}{\partial \mathbf{C}} + \phi\,\frac{\partial \psi_{chain}}{\partial \mathbf{C}}\right) = 2\left((1 - \phi)\,\frac{\partial \psi_{bulk}}{\partial I_i}\frac{\partial I_i}{\partial \mathbf{C}} + \phi\,\frac{\partial \psi_{chain}}{\partial I_i}\frac{\partial I_i}{\partial \mathbf{C}}\right) \tag{20}$$

while the First Piola-Kirchhoff stress tensor (or nominal stress tensor) is defined as follows (Holzapfel, 2000):

$$\mathbf{P} = \mathbf{F}\mathbf{S} \tag{21}$$

The nominal stress corresponds to the current force divided by the initial cross section and is therefore the typical stress measure reported in traction experiments.

If one denotes $\Im = \{I_1, I_3, I_4\}$ as the vector of invariants one can express $\mathbf{P}$ as follows:

$$\mathbf{P} = 2\sum_{i=1}^{3}\left((1 - \phi)\,\frac{\partial \psi_{bulk}}{\partial \Im_i} + \phi\,\frac{\partial \psi_{chain}}{\partial \Im_i}\right)\mathbf{F}\mathfrak{B}_i^{\mathbf{S}} \tag{22}$$

where $\mathfrak{B}_i^{\mathbf{S}}$ are the integrity bases of the material symmetry group in the reference configuration defined by their set $\mathfrak{B}^{\mathbf{S}}$:

$$\mathfrak{B}^{\mathbf{S}} = \{\mathfrak{B}_1^{\mathbf{S}}, \mathfrak{B}_3^{\mathbf{S}}, \mathfrak{B}_4^{\mathbf{S}}\} = \frac{\partial \Im}{\partial \mathbf{C}} = \{\mathbf{I}, I_3\mathbf{C}^{-1}, \cdots_0\} \tag{23}$$

The generic expression of the nominal stress tensor for the deformation invariants considered in the current formulation is:

$$\mathbf{P} = 2\left[\left((1 - \phi)\frac{\partial \psi_{bulk}}{\partial I_1} + \phi\,\frac{\partial \psi_{chain}}{\partial I_1}\right)\mathbf{F} + \phi\,\frac{\partial \psi_{chain}}{\partial I_4}\mathbf{F}\mathbf{\Lambda}_0 + (1 - \phi)I_3\frac{\partial \psi_{bulk}}{\partial I_3}\mathbf{F}^{-\mathrm{T}}\right] \tag{24}$$

To fully characterise the stress response of the material the derivatives of the strain energy function $\psi(I_1, I_3, I_4)$ must be calculated. They are provided in the **Appendix** section.

3.3 Constitutive identification procedure

The electro-spun polymer scaffold sample was tested along the original longitudinal and circumferential directions of the electro-spun hollow cylinder (**Figure 3**). In order to identify the constitutive parameters with the experimental response of the biodegradable polymer scaffold structure to circumferential and longitudinal stretches, it is necessary to establish analytical expressions of the corresponding nominal stresses (provided in the **Appendix** section). These analytical expressions are then used to perform a non-linear fitting procedure with inequality and equality constraints (see **Appendix** for a description of the objective function). Results of the identification procedure are presented in **Figure 9** by overlaying the theoretical nominal stress in the fibre and cross-fibre directions over the experimentally obtained stress. The goodness of fit between the theoretical and experimental stress is assessed using the correlation coefficient. In an earlier study it was found that degradation did not affect electrospun fibre orientation (Krynauw et al., 2011). Consequently, the parameter ρ controlling the degree of anisotropy which was determined for the non-degraded sample was fixed ($\rho = 1.27013$) for the other identification procedures (time = 4 to 28 days). Computational optimisation tests were conducted to ascertain which parameters are affected by hydrolytic degradation.

4. Results

4.1 Physical experiments

Morphology of fibrous scaffold

Scaffold porosity was 76 ± 2 %. The fibre diameter of the non-degraded scaffold was 7.37 ± 2.41 µm. The fibre alignment is illustrated in **Figure 5**, indicating predominant fibre alignment in the circumferential direction of the tubular scaffold. **Figure 5** provides SEM micrographs of the fibrous scaffold before degradation (T = 0 day) and after 7, 14 and 28 days of hydrolytic degradation. Compared to the non-degraded scaffold, increasing roughness of the fibre surfaces was observed with increasing degradation time (see **Figure 6**).

Mechanical properties

Samples of the bulk material had the dimensions of 7.2 ± 0.1 × 23.3 ± 2.9 × 0.67 ± 0.02 mm (width × length × thickness) and provided a test gauge length of 17.3 ± 2.5 mm. The fibrous scaffold samples had dimensions of 10.0 ± 0.6 × 20.0 ± 0.0 × 0.800 ± 0.004 mm providing a gauge length for tensile testing of 11.9 ± 1.3 mm.

Stress-strain data from uniaxial tensile tests of the non-degraded bulk material are presented in **Figure 7**. The bulk material exhibited a maximum stress $\sigma_{\max}$ = 2.33 ± 0.16 MPa and the associated maximum strain $\varepsilon_{\max}$ = 45.57% ± 12.72%. The uniaxial stress-strain data from orthogonal tensile test of non-degraded and degraded electro-spun scaffold are presented in **Figure 8**. Throughout the whole degradation period, $\sigma_{\max}$ and $\varepsilon_{\max}$ decreased significantly with respect to their initial value at T = 0 days. In the circumferential direction, $\sigma_{\max}$, reduced from 1.02 ± 0.23 MPa, to 0.38 ± 0.004 MPa and the associated strain, $\varepsilon_{\max}$, reduced from 46 ± 11 to 12 ± 2 %. In the longitudinal direction, $\sigma_{\max}$, reduced from 0.071 ± 0.016 MPa to 0.01 ± 0.007 MPa, and $\varepsilon_{\max}$ reduced from 69 ± 24 to 8 ± 2 %, see **Table 1.**

During the first 14 days of degradation, the ultimate stresses and strains decreased considerably (in both the longitudinal and circumferential scaffold direction). Thereafter, changes between the stress-strain curves were less considerable. The elastic modulus E was found to range between 5.57 ± 1.29 MPa and 3.85 ± 0.84 MPa in the circumferential direction and between 0.15 ± 0.08 MPa and 0.08 ± 0.04 MPa in the longitudinal direction. Differences of the elastic modulus between the degradation time points were found not to be statistically significant in either direction (p>0.05).

Molecular weight

The weight-average molecular weight (M_w) of the DegraPol® samples decreased during the degradation from 77.6 ± 5.7 kDa prior to degradation (T = 0 days, n = 3) to 51.3 ± 3.5 kDa (T = 7 days, n = 3), 41.4 ± 1.2 kDa (T = 14 days, n = 2), 33.1 ± 4.0 kDa (T = 21 days, n = 3) and 26.1 ± 6.7 kDa (T = 28 days, n = 3).

4.2 Constitutive parameters

Several identification procedures for each experimental data set (corresponding to a specific degradation time) were conducted. In the first stage, constitutive parameters for the non-degraded scaffold material (T = 0 day) were determined. The anisotropy coefficient ρ was subsequently kept constant for the identification at different degradation times based on the observation that anisotropy of electro-spun fibre scaffolds is not affected by water-induced degradation (Krynauw et al., 2011).

After a number of computational identification experiments it was found that the constitutive parameters β and p could also be fixed, meaning that they are not affected by degradation. Two of the parameters of the Knowles strain energy function, c_1 and c_2 as well as the fibre volume fraction ϕ were sensitive to degradation and they had to be allowed to vary during identification procedures at different degradation times. Fixing the volume fraction resulted in an over-prediction of the cross-fibre response. **Figure 9** provides graphs of the theoretical stress-strain curves based on the identified constitutive parameters overlaid on the original experimental data. The constitutive parameters of the transversely isotropic material model obtained for the fibrous scaffold at various degradation time points are summarised in **Table 2** as well as coefficients of determination resulting from the fitting procedure. To assess the evolution of each constitutive parameters as a function of degradation time, a relative variation metric was defined as the ratio of each parameter c_1, c_2 and ϕ over their value at 0 day degradation time (**Figure 10**).
The microstructurally-based continuum model is able to capture very well the characteristic stress response of the biodegradable polymer scaffold in the fibre and cross-fibre direction at various stages of degradation. For the transverse isotropic response the coefficients of determination were greater than 0.999 for all degradation times considered while values ranged from 0.871 to 0.999 for the isotropic response (cross-fibre plane) (see **Table 2**). Comparing the stress-strain curves to those of the reference non degraded scaffold (T = 0 day) clearly reveals a stress softening effect. The theoretical model tends to over predict the stress response in the cross-fibre direction at the more extreme strain values of few degradation times (14 % at times T = 7, 11; 11 % at times T = 28). The shape of the strain-stress curve along the fibre direction is controlled by the parameter p (see equation (3)). Experimental data showed that this parameter could be maintained constant across degradation times. During the identification procedures it was also found that the bulk compressibility parameter β is not affected by hydrolytic degradation. The key parameters affected by degradation are c_1 which controls the shear properties of the fibre and bulk material, c_2 which scales the shear response of the polymeric fibres and the fibre volume fraction ϕ. Evolution of parameters c_1, c_2 and ϕ is a non-monotonous function of degradation time (**Figure 10**). However, a simple linear regression between these parameters and degradation times exhibits an interesting trend, namely an increase with degradation time.

5. Discussion

Biodegradable scaffolds are designed as temporary structures for tissue regeneration therapies. Suitable physical, chemical and mechanical properties of the scaffold tailored to a specific application are essential requirements for the clinical success of the scaffold and therapy. In this context, knowledge of the mechanical properties and how they are affected by the degradation is crucial for successful scaffold design. In this study, we mechanically characterised electro-spun fibrous scaffolds of a biodegradable polyester-urethane during hydrolytic *in vitro* degradation of up to 28 days. We subsequently developed a microstructurally-motivated continuum constitutive law that closely predicts the mechanical transverse isotropy of the scaffold with a high degree of fibre alignment. Although featuring a limited number of parameters (5 + fibre volume fraction), the constitutive formulation exhibits enough universality to capture the effects of degradation on the mechanical properties of the scaffold through only three parameters.

Investigating structural changes due to water penetration into the scaffolds during hydrolytic degradation is fundamental for understanding the rate and mechanism of degradation which affect the mechanical properties of the scaffold. Consistent with earlier results (Krynauw et al., 2011), fibre fracture and pitting were not apparent during degradation period of up to 28 days. The SEM images showed an increase in the surface roughness of the fibres during degradation. The reason behind this is not fully understood. Surface roughness of electro-spun fibres has been addressed widely (Milleret et al., 2012; Sawawi et al., 2013) and ascribed to process conditions during electro-spinning such as humidity, polymer concentration, and the type of solvent used (Casper et al., 2003; Pai et al., 2009). Increase in the surface roughness of the fibres after onset of degradation in PBS solution at 37°C has been reported for electro-spun poly(lactic-co-glycolic acid) (Duan et al., 2007) and DegraPol® (Henry et al., 2007) scaffolds. However, none of these studies dealt with it as an obvious morphological change.

The loss of the mechanical strength of the polymer with degradation is a substantial indicator of polymer degradation. Preliminary tensile tests with degraded samples indicated that load cycling was not feasible without inducing substantial damage prior to the final loading due to loss in mechanical properties, in particular at longer degradation time points. Hence, cycling was not included in the tensile test protocol and samples were loaded to failure with the first loading. Over 28 days of degradation, the scaffold experienced a considerable decrease in the maximum stress and the associated strain of 62.7% and 78.3%, respectively, in circumferential direction and of 88.7% and 88.4%, respectively, in longitudinal direction. The decrease of maximum stress and strain was larger during the first 14 days of degradation compared to the changes observed between day 14 and 28 of degradation.

The change in the mechanical properties during the degradation period can be explained by the hydrolysis procedure of the segmented structure of PU-based materials such as DegraPol®, which is highly influenced by the chemical composition and the molecular organization of the material. As the Degrapol® contains three different hydrolytically degradable esters in its hard and soft segments, the differential degradation rates of the components due to chemistry and position (soft vs. hard segment) may account for the apparent slow-down in degradation (as evidenced by the decrease in mechanical properties).

The ability of the scaffold to maintain its elastic properties during degradation is a desired quality for tissue regeneration, as many tissues demand a certain elastic modulus to be able to thrive and differentiate (Shoichet, 2009). A stable elastic modulus allows the scaffold to keep mechanical integrity and provide mechanical support until new tissue formation and healing occurs. In agreement with Henry et al. (2007), our results did not show significant change in the elastic modulus of electro-spun DegraPol® scaffolds during the entire degradation period. Generally, the elastic properties of polyurethanes are dominated by the crystalline segment of the polymer (Borkenhagen et al., 1998; Henry et al., 2007), referred to as hard segments, which contains the degradable urethane groups (Basak and Adhikari, 2013). It appears that due to its crystalline arrangements, hard segments show less accessibility to biodegradation (Umare and Chandure, 2008), hence any significant change in the elastic modulus during the degradation period was not observed. In fact some studies have reported that urethane bonds are only enzymatically degraded (Hafeman et al., 2011; Shi et al., 2009). Investigating the mass loss and molecular weight reduction during the degradation can add considerably to understanding the degradation mechanism of DegraPol®. The results show that the mass loss during the 28 days of degradation was approximately 2% while the molecular weight reduction was about 58%. The significant reduction in the molecular weight prior to significant mass loss represents a typical bulk erosion mechanism which resulted in the cleavage of the ester bonds within the polymer and causing the mechanical strength loss.
The cleavage of the ester bonds resulted in the formation of fragments which were still too large to be released from the bulk during the degradation period and hence merely a slight decrease in the scaffold mass during the degradation period was observed which, on the other hand could have been induced by the limited degradation that has occurred in the polymer surface as can be seen from the SEM micrographs of the degraded samples. Similar results were reported by Kylmä and Seppälä (1997) who observed significant reduction in the molecular weight of a series of polyester-urethane after exposure to PBS whereas no significant change in the polymer mass was detected until 30 days of degradation when the molecular weight of the polymer has decreased sufficiently. It appears that, in the region studied, the relationship between $\ln(M_n)$ and the degradation time follows a linear relationship as proposed by Farrar and Gillson (2002) for polyesters and their co-polymers, where the M_n of the polymer is related to the degradation time through the relationship.

$$M_n = M_{n,0} e^{-kT} \tag{25}$$

where $M_{n,0}$ is the initial number average molecular weight of the polymer, k is a constant and T is the degradation time.

Three constitutive parameters only (c_1, c_2 and ϕ) were required to capture alterations of mechanical properties of the scaffold material over a 28 days hydrolysis period These parameters represent the mechanical properties of the bulk material composing the electro-spun polymer fibres and their volume fraction. Although the constitutive behaviour of the bulk material DegraPol® is fully defined by three parameters, c_1, c_2 and p, the latter which only controls the shape of the stress-strain curve is not affected by hydrolysis (**Figure 7** and **Figure 8**. The parameter β which controls the compressibility of the scaffold material (not that of the polymeric fibres) was maintained constant during the identification procedures as the assumption of incompressibility.
However, the mean scaffold porosity of the degraded and non-degraded samples was measured as 76% and this would suggest some degree of compressibility. This means that the assumption of macroscopic incompressibility represents a potential limitation of the current identification procedure with the experimental tensile test data that were collected. Compressibility could have been determined by calculating the lateral stretches from the lateral contractions of the sample. In a state of homogeneous uniaxial deformations, the determinant of the deformation gradient—which maps an infinitesimal element volume from the undeformed to the deformed configuration—is is simply the product of the three principal stretches. Lateral contraction of the samples were not measured during the tensile test and so could not be inferred later without using inverse finite element-based identification which was out of the scope of the present work. Accounting for the compressibility of the sample would likely affect the identified parameters but would be unlikely to impair the ability of the constitutive model to model the mechanical behaviour of the scaffold material.

The mean free gauge length for testing of the samples was 11.9 mm at a mean width of 10 mm. This gives a length to width aspect ratio of about 1.2, which is unlikely to induce a state of homogeneous uniaxial tension in the clamped specimen. However, for parameter identification and for sake of tractability/practicality, the analytic solution for the homogeneous uniaxial tension case was used. In order to assess the effect of this assumption, the transversely isotropic hyperelastic constitutive model was implemented in a finite element code so that solutions for non-homogeneous deformations could be calculated. Two cases were simulated: 15% strain uniaxial extension for **homogeneous** deformations (perfect homogeneous conditions which do not introduce parasitic shear) and 15% uniaxial extension for **non-homogeneous** deformations (the two end faces of the 3D sample were assumed to be rigid). The relative error for the relevant stress component between homogeneous and non-homogeneous deformations (measured at the centre of the sample) varies between 5.65 and 13.81% along the fibre direction (**Figure 1**) and 16.60 and 25.61% in the direction transverse to the fibre (**Figure 2**). These results indicate that the mechanical properties that were experimentally measured and from which constitutive parameters were subsequently identified are overestimated. However, the stress responses are qualitatively identical for homogeneous and non-homogeneous deformations. The quantitative discrepancy is a present limitation of the experimental data set and future experimental characterisation should ensure states of purely uniaxial tension in the specimens. Alternatively, identification of constitutive parameters based on inverse finite element analysis procedures (featuring non-homogeneous states of deformation) could have been used. This is beyond the scope of the current work. The main focus of this research concerns the formulation of a simple constitutive model capable of faithfully (at least qualitatively) capturing the macroscopic behaviour of electros-spun polymer fibre scaffold.

The fact that the variations of c_1 and c_2 (all positive parameters) appear to follow a similar trend (**Figure 10**) is consistent with the assumption that the material making up the electro-spun fibres experiences a change in its mechanical properties. At 4 days degradation time, c_1 increases by about 40% (**Figure 10**-a) whilst the corresponding change in c_2 exceeds 80%. However, inconsistencies between degradation time and reduction in mechanical properties are not byproducts of the identification procedure but rather present in the original experimental measurements. For example compare the apparent stiffness of the material at 5% strain at 0 and 4 days degradation time (**Figure 9**). Roughening of the surface of polymer fibres observed through SEM imaging (**Figure 5**) implies a deposition or resorption of material as a result of hydrolysis. This physical process could play a role in affecting the structural response of the scaffold so that weakening or even strengthening of it could result.

The fibre volume fraction ϕ increases with degradation time (**Figure 10**-c) and appears to follow a similar trend to c_2, and to a certain extent, c_1. During the numerical identification of the constitutive parameters, equal weights were assigned to the squared differences for the fibre and cross-fibre data entering the definition of the objective function (**Appendix**). That means that no particular direction (either fibre or cross-fibre) was favoured in the optimisation of parameters. However, given the large ratio of stiffness of the two directions in combination with the minimisation of a least-square function, a bias was introduced towards the stress-strain curve in the fibre direction. This is a possible explanation for the model overprediction of the cross-fibre stress-strain described in section **4.2**. However, the main point to make here is that, an increase in the fibre volume fraction (**Figure 10**-c) would imply an increase of the mechanical dominance of the fibre over the cross-fibre direction. This is a consequence of the identification procedure but could equally be caused by the progressive degradation of the polymer bulk aggregates interacting with the polymer fibres.

The focus of constitutive model presented here was on capturing the non-linear transversely isotropic behaviour of electro-spun biodegradable polymer scaffolds with a high degree of fibre alignment at various stages of hydrolysis-induced degradation. Although phenomenological in nature, the constitutive formulation incorporates microstructural features such as the use of a microscopic unit cell affinely deforming under the influence of macroscopic loads (Arruda and Boyce, 1993; Kuhl et al., 2005). The use of a 8-chain conformation induces network properties which can be transversely isotropic thanks to the introduction of two characteristic lengths for the unit cell (Kuhl et al., 2005).

In the definition of the bulk energy of the electro-spun scaffold material, the shear modulus-like parameter c_1 was also used for the definition of the strain energy function characterising the elasticity of polymer fibres (18). This assumption ensures that the phenomenological microstructurally-based constitutive law has a physical interpretation in relation to the bulk properties of the biodegradable polymer by linking the mechanical properties of individual fibres to that of the (macroscopic) scaffold. This is an efficient compromise between a fully-fledged micromechanical model explicitly capturing the geometry and mechanics of individual polymer fibres (D'Amore et al., 2014) and a purely phenomenological model ignoring any structural aspects of the scaffold.

The main limitation of the proposed constitutive model is that it does not explicitly capture the inelastic behaviour of the scaffold in terms of water-induced degradation (Soares et al., 2007; Soares et al., 2010c; Soares and Zunino, 2010b; Vieira et al., 2011), viscoelastic (Muliana and Rajagopal, 2012a) and viscoplastic behaviour (Khan and El-Sayed, 2013; Vieira et al., 2014) and mechanical damage due to excessive loading (Soares, 2008). Such features will no doubt augment the fidelity of the material modelling and increase predictive capabilities by providing a mechanistic link between degradation time and resulting altered mechanical properties.

The 8-chain microstructural framework proposed here could be extended to account for these mechanical behaviours by modifying the constitutive formulation defining the behaviour of polymer fibres and that of the bulk scaffold material (equations (3) and (12)). The transversely isotropic 8-chain conformation would remain identical in terms of kinematics. Alternatively, one could use the model proposed by Vieira et al. (2014) and extend it to transverse isotropy by introducing a second characteristic dimension in the unit cell of the 8-chain model (Bischoff et al., 2002b, c; Kuhl et al., 2005). Instead of using a chain energy based on entropic elasticity (defined by configurational entropy rather than internal energy) of macromolecules one could also adopt a similar ansatz to what is proposed in our model, namely a bimodal Knowles strain energy function (null in compression along the fibre direction). The present model enjoys a simple formulation featuring a limited number of constitutive parameter and can capture variations of elastic mechanical properties for moderate strain levels as a result of progressive water-induced damage.

6. Conclusion

We have characterised the non-linear transversely isotropic elastic tensile behaviour of electro-spun biodegradable polyester-urethane scaffolds intended for cardiovascular tissue regeneration at various stages of water-induced degradation over a 28 days period via tensile tests. The stress-strain data at 0, 4, 7, 11, 14, 17, 21, 24 and 28 days were used to identify parameters of a new 3D transversely isotropic continuum constitutive formulation. Mechanical testing was complemented by SEM imaging which, apart from roughening of the surface of polymer fibres, no major structural alteration of the scaffold was observed. The microstructurally-motivated phenomenological constitutive model is based on the definition of a microscopic unit cell which features two distinct characteristic lengths and account for the non-linear mechanics of polymer fibres arranged in a non-isotropic 8-chain conformation. Despite its simplicity and limited number of parameters the constitutive formulation can accurately reproduce the stress-strain response of highly aligned electro-spun biodegradable polymer scaffolds at up to 28 days degradation time. Degradation of the macroscopic mechanical properties of the scaffold are faithfully accounted for by only three constitutive parameters.

7. Acknowledgments

The authors thank ab medica S.p.A for donating the DegraPol® material for this study. ETH Zurich and the University of Zurich are owners and ab medica S.p.A is exclusive licensee of all Intellectual Property Rights of DegraPol®. This study was supported financially by a Royal Society International Exchange grant [#IE120555] to Georges Limbert and Thomas Franz, and the National Research Foundation (NRF) of South Africa. Any opinion, findings and conclusions or recommendations expressed in this publication are those of the authors and therefore the NRF does not accept any liability in regard thereto. The development of the constitutive model was initiated during a visit of Georges Limbert to the University of Cape Town supported by the World Universities Network. Thomas Franz was awarded a Distinguished Visiting Fellowship from the Royal Academy of Engineering (UK) and a Researcher Mobility Award from the World Universities Network for visits to the University of Southampton. Hugo Krynauw received a matching dissertation grant from the International Society of Biomechanics. All the funding sources are gratefully acknowledged.

8. Conflict of interest statement

The authors declare that they do not have conflicts of interest with regard to this manuscript and the data presented therein.

9. References

Arruda, E.M., Boyce, M.C., 1993. A three-dimensional constitutive model for the large stretch behavior of rubber elastic-materials, J Mech Phys Solids 41, 389-412.

Ayres, C.E., Bowlin, G.L., Henderson, S.C., Taylor, L., Shultz, J., Alexander, J., Telemeco, T.A., Simpson, D.G., 2006. Modulation of anisotropy in electrospun tissue-engineering scaffolds: Analysis of fiber alignment by the fast Fourier transform, Biomaterials 27, 5524-5534.

Ayres, C.E., Bowlin, G.L., Pizinger, R., Taylor, L.T., Keen, C.A., Simpson, D.G., 2007. Incremental changes in anisotropy induce incremental changes in the material properties of electrospun scaffolds, Acta Biomaterialia 3, 651-661.

Ayres, C.E., Jha, B.S., Meredith, H., Bowman, J.R., Bowlin, G.L., Henderson, S.C., Simpson, D.G., 2008. Measuring fiber alignment in electrospun scaffolds: a user's guide to the 2D fast Fourier transform approach, Journal of Biomaterials Science, Polymer Edition 19, 603-621.

Basak, P., Adhikari, B., 2013. Biodegradation of Polyester Urethane in Simulated Body Fluid, Polymer-Plastics Technology and Engineering 52, 358-367.

Bergstrom, J.S., Boyce, M.C., 1998. Constitutive modeling of the large strain time-dependent behavior of elastomers, J Mech Phys Solids 46, 931-954.

Bischoff, J.E., Arruda, E.A., Grosh, K., 2002a. A microstructurally based orthotropic hyperelastic constitutive law, J Appl Mech 69, 570-579.

Bischoff, J.E., Arruda, E.M., Grosh, K., 2002b. Finite element simulations of orthotropic hyperelasticity, Finite Elem. Anal. Des. 38, 983-998.

Bischoff, J.E., Arruda, E.M., Grosh, K., 2002c. Orthotropic hyperelasticity in terms of an arbitrary molecular chain model, J Appl Mech 69, 198-201.

Boehler, 1978. Lois de comportement anisotrope des milieux continus, Journal de Mécanique 17, 153-190.

Borkenhagen, M., Stoll, R.C., Neuenschwander, P., Suter, U.W., Aebischer, P., 1998. In vivo performance of a new biodegradable polyester urethane system used as a nerve guidance channel, Biomaterials 19, 2155-2165.

Braghirolli, D.I., Steffens, D., Pranke, P., 2014. Electrospinning for regenerative medicine: a review of the main topics, Drug Discov Today 19, 743-753.

Casper, C.L., Stephens, J.S., Tassi, N.G., Chase, D.B., Rabolt, J.F., 2003. Controlling Surface Morphology of Electrospun Polystyrene Fibers: Effect of Humidity and Molecular Weight in the Electrospinning Process, Macromolecules 37, 573-578.

Chandran, P.L., Barocas, V.H., 2006. Affine versus non-affine fibril kinematics in collagen networks: Theoretical studies of network behavior, J Biomech Eng 128, 259-270.

Chen, Y.H., Li, Q., 2010. Mathematical modeling of polymer biodegradation and erosion, Pricm 7, Pts 1-3 654-656, 2071-2074.

Chen, Y.H., Zhou, S.W., Li, Q., 2011. Mathematical modeling of degradation for bulk-erosive polymers: Applications in tissue engineering scaffolds and drug delivery systems, Acta Biomater 7, 1140-1149.

Courtney, T., Sacks, M.S., Stankus, J., Guan, J., Wagner, W.R., 2006. Design and analysis of tissue engineering scaffolds that mimic soft tissue mechanical anisotropy, Biomaterials 27, 3631-3638.

D'Amore, A., Amoroso, N., Gottardi, R., Hobson, C., Carruthers, C., Watkins, S., Wagner, W.R., Sacks, M.S., 2014. From single fiber to macro-level mechanics: A structural finite-element model for elastomeric fibrous biomaterials, J Mech Behav Biomed Mater 39, 146-161.

Dargaville, B.L., Vaquette, C., Rasoul, F., Cooper-White, J.J., Campbell, J.H., Whittaker, A.K., 2013. Electrospinning and crosslinking of low-molecular-weight poly(trimethylene carbonate-co-l-lactide) as an elastomeric scaffold for vascular engineering, Acta Biomater 9, 6885-6897.

Duan, B., Wu, L., Li, X., Yuan, X., Li, X., Zhang, Y., Yao, K., 2007. Degradation of electrospun PLGA-chitosan/PVA membranes and their cytocompatibility in vitro, Journal of Biomaterials Science, Polymer Edition 18, 95-115.

Farrar, D.F., Gillson, R.K., 2002. Hydrolytic degradation of polyglyconate B: the relationship between degradation time, strength and molecular weight, Biomaterials 23, 3905-3912.

Fung, Y.C., 1981. Biomechanics: mechanical properties of living tissues. Springer-Verlag, New York.

Furth, M.E., Atala, A., van Dyke, M.E., 2007. Smart biomaterials design for tissue engineering and regenerative medicine, Biomaterials 28, 5068-5073.

Grabow, N., Bunger, C.M., Schultze, C., Schmohl, K., Martin, D.P., Williams, S.F., Sternberg, K., Schmitz, K.P., 2007. A biodegradable slotted tube stent based on Poly(L-lactide) and poly(4-hydroxybutyrate) for rapid balloon-expansion, Ann Biomed Eng 35, 2031-2038.

Grabow, N., Wentzlaff, M., Senz, V., Seidlitz, A., Harder, C., Sternberg, K., Weitschies, W., Schmitz, K.P., 2013. Feasibility of Polymer/Drug Coating on Absorbable and Permanent Stent Platforms - Technological Challenges, Biomed Eng-Biomed Te 58.

Hafeman, A.E., Zienkiewicz, K.J., Zachman, A.L., Sung, H.-J., Nanney, L.B., Davidson, J.M., Guelcher, S.A., 2011. Characterization of the degradation mechanisms of lysine-derived aliphatic poly(ester urethane) scaffolds, Biomaterials 32, 419-429.

Hatami-Marbini, H., Picu, R.C., 2009. An eigenstrain formulation for the prediction of elastic moduli of defective fiber networks, Eur. J. Mech. A-Solids 28, 305-316.

Henry, J.A., Simonet, M., Pandit, A., Neuenschwander, P., 2007. Characterization of a slowly degrading biodegradable polyesterurethane for tissue engineering scaffolds, Journal of Biomedical Materials Research Part A 82A, 669-679.

Holzapfel, G.A., 2000. Nonlinear Solid Mechanics. A Continuum Approach for Engineering. John Wiley & Sons, Chichester, UK.

Holzapfel, G.A., Gasser, T.C., Ogden, R.W., 2000. A new constitutive framework for arterial wall mechanics and a comparative study of material models, J Elast 61, 1-48.

Humphrey, J.D., Yin, F.C.P., 1987. On constitutive relations and finite deformations of passive cardiac tissue: I: "A pseudostrain energy function", J Biomech Eng 109, 298-304.

Khan, K.A., El-Sayed, T., 2013. A phenomenological constitutive model for the nonlinear viscoelastic responses of biodegradable polymers, Acta Mechanica 224, 287-305.

Knowles, J.K., 1977. Finite anti-plane shear field near tip of a crack for a class of incompressible elastic solids, Int. J. Fract. 13, 611-639.

Kratky, O., Porod, G., 1949. Röntgenuntersuchungen gelöster Fadenmoleküle, Rec Trav Chim Pays-Bas Belg 68, 1106-1122.

Krynauw, H., Bruchmüller, L., Bezuidenhout, D., Zilla, P., Franz, T., 2011. Degradation-induced changes of mechanical properties of an electro-spun polyester-urethane scaffold for soft tissue regeneration, Journal of Biomedical Materials Research Part B: Applied Biomaterials 99B, 359-368.

Kuhl, E., Garikipati, K., Arruda, E., Grosh, K., 2005. Remodeling of biological tissue: Mechanically induced reorientation of a transversely isotropic chain network, J Mech Phys Solids 53, 1552-1573.

Kylmä, J., Seppälä, J.V., 1997. Synthesis and Characterization of a Biodegradable Thermoplastic Poly(ester−urethane) Elastomer, Macromolecules 30, 2876-2882.

Limbert, G., 2011. A mesostructurally-based anisotropic continuum model for biological soft tissues--Decoupled invariant formulation, J Mech Behav Biomed Mater 4, 1637-1657.

Limbert, G., Taylor, M., 2002. On the constitutive modeling of biological soft connective tissues. A general theoretical framework and tensors of elasticity for strongly anisotropic fiber-reinforced composites at finite strain, Int J Solids Struct 39, 2343-2358.

Marsden, J.E., Hughes, T.J.R., 1994. Mathematical Foundations of Elasticity. Dover, New-York.

Milleret, V., Hefti, T., Hall, H., Vogel, V., Eberli, D., 2012. Influence of the fiber diameter and surface roughness of electrospun vascular grafts on blood activation, Acta Biomaterialia 8, 4349-4356.

Milleret, V., Simonet, M., Bittermann, A.G., Neuenschwander, P., Hall, H., 2009. Cyto- and hemocompatibility of a biodegradable 3D-scaffold material designed for medical applications, J Biomed Mater Res B Appl Biomater 91, 109-121.

Moore, J.E., Soares, J.S., Rajagopal, K.R., 2010. Deformation-induced hydrolysis of a degradable polymeric cylindrical annulus, Biomech Model Mechanobiol 9, 177-186.

Muliana, A., Rajagopal, K.R., 2012a. Modeling the response of nonlinear viscoelastic biodegradable polymeric stents, Int J Solids Struct 49, 989-1000.

Muliana, A., Rajagopal, K.R., 2012b. On the response of viscoelastic biodegradable polymeric solids, Mech Res Commun 39, 51-58.

Ogden, R.W., 1984. Non-Linear Elastic Deformations. Ellis Horwood Ltd., West Sussex, England.

Pai, C.-L., Boyce, M.C., Rutledge, G.C., 2009. Morphology of Porous and Wrinkled Fibers of Polystyrene Electrospun from Dimethylformamide, Macromolecules 42, 2102-2114.

Pence, T.J., Monroe, R.J., Wright, N.T., 2008. On the computation of stress in affine versus nonaffine fibril kinematics within planar collagen network models, J Biomech Eng 130.

Riboldi, S.A., Sampaolesi, M., Neuenschwander, P., Cossu, G., Mantero, S., 2005. Electrospun degradable polyesterurethane membranes: potential scaffolds for skeletal muscle tissue engineering, Biomaterials 26, 4606-4615.

Rizvi, M.S., Pal, A., 2014. Statistical model for the mechanical behavior of the tissue engineering non-woven fibrous matrices under large deformation, J Mech Behav Biomed Mater 37, 235-250.

Rocco, K.A., Maxfield, M.W., Best, C.A., Dean, E.W., Breuer, C.K., 2014. In Vivo Applications of Electrospun Tissue-Engineered Vascular Grafts: A Review, Tissue Engineering Part B: Reviews.
Roh, J.D., Nelson, G.N., Brennan, M.P., Mirensky, T.L., Yi, T., Hazlett, T.F., Tellides, G., Sinusas, A.J., Pober, J.S., Saltzman, W.M., Kyriakides, T.R., Breuer, C.K., 2008. Small-diameter biodegradable scaffolds for functional vascular tissue engineering in the mouse model, Biomaterials 29, 1454-1463.
Sander, E.A., Stylianopoulos, T., Tranquillo, R.T., Barocas, V.H., 2009. Image-based multiscale modeling predicts tissue-level and network-level fiber reorganization in stretched cell-compacted collagen gels, PNAS 106, 17675-17680.
Sastry, A.M., Cheng, X., Wang, C.W., 1998. Mechanics of stochastic fibrous networks, J Thermoplast Compos Mater 11, 288-296.
Sastry, A.M., Wang, C.W., Berhan, L., 2001. Deformation and failure in stochastic fibrous networks: Scale, dimension and application, Probabilistic Methods in Fatigue and Fracture 200, 229-250.
Sawawi, M., Wang, T.Y., Nisbet, D.R., Simon, G.P., 2013. Scission of electrospun polymer fibres by ultrasonication, Polymer.
Shi, R., Chen, D., Liu, Q., Wu, Y., Xu, X., Zhang, L., Tian, W., 2009. Recent Advances in Synthetic Bioelastomers, International Journal of Molecular Sciences 10, 4223-4256.
Shoichet, M.S., 2009. Polymer Scaffolds for Biomaterials Applications, Macromolecules 43, 581-591.
Silberstein, M.N., Pai, C.-L., Rutledge, G.C., Boyce, M.C., 2012. Elastic–plastic behavior of non-woven fibrous mats, Journal of the Mechanics and Physics of Solids 60, 295-318.
Soares, J., Rajagopal, K., Moore, J., 2010a. Deformation-induced hydrolysis of a degradable polymeric cylindrical annulus, Biomech Model Mechanobiol 9, 177-186.
Soares, J.S., 2008. Constitutive modeling for biodegradable polymers for applications in endovascular stents, Mechanical Engineering Department, Texas A&M.
Soares, J.S., Moore, J.E., Rajagopal, K.R., 2007. Constitutive model of biodegradable, non-linear polymeric materials for applications in the biomedical field, Proceeding of the ASME Summer Bioengineering Conference - 2007, 733-734.
Soares, J.S., Moore, J.E., Rajagopal, K.R., 2010b. Modeling of Deformation-Accelerated Breakdown of Polylactic Acid Biodegradable Stents, J Med Devices 4.
Soares, J.S., Rajagopal, K.R., Moore, J.E., 2010c. Deformation-induced hydrolysis of a degradable polymeric cylindrical annulus, Biomech Model Mechanobiol 9, 177-186.
Soares, J.S., Zunino, P., 2010a. A mixture model for water uptake, degradation, erosion and drug release from polydisperse polymeric networks, Biomaterials 31, 3032-3042.
Soares, J.S., Zunino, P., 2010b. A Multiscale Mixture Model for Polymer Degradation and Erosion, Proceedings of the Asme Summer Bioengineering Conference, 2010, 113-114.
Spencer, A.J.M., 1992. Continuum theory of the mechanics of fibre-reinforced composites. Springer-Verlag, New York.
Stella, J.A., Wagner, W.R., Sacks, M.S., 2010. Scale-dependent fiber kinematics of elastomeric electrospun scaffolds for soft tissue engineering, Journal of Biomedical Materials Research Part A 93A, 1032-1042.
Stylianopoulos, T., Bashur, C.A., Goldstein, A.S., Guelcher, S.A., Barocas, V.H., 2008. Computational predictions of the tensile properties of electrospun fibre meshes: Effect of fibre diameter and fibre orientation, J Mech Behav Biomed Mater 1, 326-335.
Umare, S.S., Chandure, A.S., 2008. Synthesis, characterization and biodegradation studies of poly(ester urethane)s, Chemical Engineering Journal 142, 65-77.
Vieira, A.C., Guedes, R.M., Tita, V., 2014. Constitutive modeling of biodegradable polymers: Hydrolytic degradation and time-dependent behavior, Int J Solids Struct 51, 1164-1174.
Vieira, A.C., Medeiros, R., Guedes, R.M., Marques, A.T., Tita, V., 2013. Visco-Elastic-Plastic Properties of Suture Fibers Made of PLA-PCL, Advanced Materials Forum Vi, Pts 1 and 2 730-732, 56-61.
Vieira, A.C., Vieira, J.C., Ferra, J.M., Magalhaes, F.D., Guedes, R.M., Marques, A.T., 2011. Mechanical study of PLA-PCL fibers during in vitro degradation, J Mech Behav Biomed Mater 4, 451-460.
Wang, C.W., Berhan, L., Sastry, A.M., 2000. Structure, mechanics and failure of stochastic fibrous networks: Part I - Microscale considerations, J. Eng. Mater. Technol.-Trans. ASME 122, 450-459.
Wang, C.W., Sastry, A.M., 2000. Structure, mechanics and failure of stochastic fibrous networks: Part II - Network simulations and application, J. Eng. Mater. Technol.-Trans. ASME 122, 460-468.
Williams, D.F., 2006. To engineer is to create: the link between engineering and regeneration, Trends Biotechnol 24, 4-8.

Wu, H., Fan, J., Chu, C.-C., Wu, J., 2010. Electrospinning of small diameter 3-D nanofibrous tubular scaffolds with controllable nanofiber orientations for vascular grafts, Journal of Materials Science: Materials in Medicine 21, 3207-3215.
Wu, X.F., Dzenis, Y.A., 2005. Elasticity of planar fiber networks, J Appl Phys 98.
Zilla, P., Bezuidenhout, D., Human, P., 2007. Prosthetic vascular grafts: Wrong models, wrong questions and no healing, Biomaterials 28, 5009-5027.

Appendix

Derivatives of the strain energy functions

Derivatives of the strain energy functions $\psi_{bulk}(I_1, I_3)$ and $\psi_{chain}(I_1, I_4)$ characterising the transversely isotropic hyperelastic model (reproduced here for convenience) are calculated.

If one denotes $\mathcal{S}$ as:

$$\mathcal{S} = \langle \lambda_r - 1 \rangle^0 = \langle \sqrt{\frac{I_4\xi_a^2 + (I_1 - I_4)\xi_b^2}{\xi_a^2 + 2\xi_b^2}} - 1 \rangle^0 \tag{26}$$

$$\psi_{chain} = \mathcal{S}\frac{c_1}{2c_2}\left[\left[1 + \frac{c_2}{p}\left(\frac{I_4\xi_a^2 + (I_1 - I_4)\xi_b^2}{\xi_a^2 + 2\xi_b^2} + 2\sqrt{\frac{\xi_a^2 + 2\xi_b^2}{I_4\xi_a^2 + (I_1 - I_4)\xi_b^2}} - 3\right)\right]^p - 1\right] \tag{27}$$

$$\psi_{bulk} = c_1\left[(I_1 - 3) + \frac{1}{\beta}(I_3^{-\beta} - 1)\right] \tag{28}$$

$$\frac{\partial \psi_{chain}}{\partial I_1} = \mathcal{S}\frac{c_1}{c_2}\left\{-1 + \left[1 + \frac{c_2\left(-3 + 2\sqrt{\frac{\xi_a^2 + 2\xi_b^2}{\xi_b^2(I_1 - I_4) + \xi_a^2 I_4}} + \frac{\xi_b^2(I_1 - I_4) + \xi_a^2 I_4}{\xi_a^2 + 2\xi_b^2}\right)}{p}\right]^p\right\} \tag{29}$$

$$\frac{\partial \psi_{chain}}{\partial I_4} = \frac{\xi_b^2 c_1 \mathcal{S}}{\xi_a^2 + 2\xi_b^2}\left[1 - \left(\frac{\xi_a^2 + 2\xi_b^2}{\xi_b^2(I_1 - I_4) + \xi_a^2 I_4}\right)^{3/2}\right]\left[1 + \frac{c_2\left(-3 + \frac{\xi_b^2(I_1 - 3I_4)}{\xi_a^2 + 2\xi_b^2} + I_4 + 2\sqrt{\frac{\xi_a^2 + 2\xi_b^2}{\xi_b^2(I_1 - I_4) + \xi_a^2 I_4}}\right)}{p}\right]^{p-1} \tag{30}$$

$$\frac{\partial \psi_{bulk}}{\partial I_1} = c_1; \frac{\partial \psi_{bulk}}{\partial I_3} = -c_1 I_3^{-(\beta+1)} \tag{31}$$

Analytical solutions for homogeneous deformations

It is assumed that the measured deformations were homogeneous so that no spurious shear coupling was introduced. In these conditions, the deformation gradient can be written as $\mathbf{F} = \lambda_x \mathbf{e}_x \otimes \mathbf{e}_x + \lambda_y \mathbf{e}_y \otimes \mathbf{e}_y + \lambda_z \mathbf{e}_z \otimes \mathbf{e}_z$ and the nominal stress tensor takes the simplified form:

$$\mathbf{P} = \left(\frac{\partial \psi}{\partial \lambda_x} - \frac{P}{\lambda_x}\right)\mathbf{e}_x \otimes \mathbf{e}_x + \left(\frac{\partial \psi}{\partial \lambda_y} - \frac{P}{\lambda_y}\right)\mathbf{e}_y \otimes \mathbf{e}_y + \left(\frac{\partial \psi}{\partial \lambda_z} - \frac{P}{\lambda_z}\right)_z \mathbf{e}_z \otimes \mathbf{e}_z \tag{32}$$

where the scalar P is identified with the pressure arising as a reaction to the incompressibility constraint.

Uniaxial extension along the longitudinal direction

For a homogeneous uniform extension λ_z along the $z - axis$ one can deduce, because of material isotropy in the $(x, y) - plane$ and volume-preserving deformations that $\lambda_x = \lambda_y$ and $\lambda_x\lambda_y\lambda_z = 1$. It follows that the the deformation gradient is:

$$\mathbf{F} = \frac{1}{\sqrt{\lambda_z}}(\mathbf{e}_x \otimes \mathbf{e}_x + \mathbf{e}_y \otimes \mathbf{e}_y) + \lambda_z \mathbf{e}_z \otimes \mathbf{e}_z \tag{33}$$

The assumption of equal lateral stretches (along $\mathbf{e}_x$ and $\mathbf{e}_y$) is an approximation as the electro-spun fibre scaffold material is not a perfect transversely isotropic material. As elaborated upon in the discussion section concerning the assumption of incompressibility this could be addressed in future studies by conducting appropriate measurements.

The nominal stress tensor takes the form:

$$\mathbf{P} = P_{zz}\mathbf{e}_z \otimes \mathbf{e}_z = \left(\frac{\partial \psi}{\partial \lambda_z} - \lambda_z^{-\frac{3}{2}}\frac{\partial \psi}{\partial \lambda_y}\right)_z \mathbf{e}_z \otimes \mathbf{e}_z = P^{\parallel}(\lambda_z)\,\mathbf{e}_z \otimes \mathbf{e}_z \tag{34}$$

The pressure P is calculated from equation and the condition of traction-free lateral directions ($x-$ and $y-axis$) ($P_{xx} = P_{yy} = 0$). It can therefore be eliminated from the expression of P_{zz}.

Uniaxial extension along the circumferential direction

Using similar arguments to those in the previous sections the nominal stress tensor takes the following form:

$$\mathbf{P} = P_{xx}\mathbf{e}_x \otimes \mathbf{e}_x = \left(\frac{\partial \psi}{\partial \lambda_x} - \lambda_x^{-\frac{3}{2}}\frac{\partial \psi}{\partial \lambda_y}\right)\mathbf{e}_x \otimes \mathbf{e}_x = P^{\perp}(\lambda_x)\,\mathbf{e}_x \otimes \mathbf{e}_x \tag{35}$$

Identification of constitutive parameters – objective function

Data from the experimental uniaxial tensile tests described in section **2.3** were used to identify sets of constitutive parameters for the prototype material law described in section **3**. Data consisted of uniaxial tensions along the main polymer fibre direction ($\bar{\lambda}_i, \bar{y}_i{}^{\parallel}$)(superscript ∥) and perpendicular to it ($\bar{\lambda}_i, \bar{y}_i{}^{\perp}$)(superscript ⊥) at various degradation times from 0 to 28 days.

$$\mathfrak{O}\,(\mathbf{p}) = \frac{1}{N}\sum_{i=1}^{N}\left(P^{\parallel}(\bar{\lambda}_i) - \bar{y}_i^{\parallel}\right)^2 + \frac{1}{M}\sum_{j=1}^{M}\left(P^{\perp}(\bar{\lambda}_j) - \bar{y}_j^{\perp}\right)^2 \tag{36}$$

where $\mathbf{p} = \{\beta, c_1, c_2, p, \rho, \phi\}$ is the vector containing the constitutive parameters. The identification process consists in finding a set of constitutive parameters that minimise the function $\mathfrak{O}\,(\mathbf{p})$ subject to specific constraints:

$$\{\beta > 0;\quad c_1 > 0;\quad c_2 > 0;\quad p > 0;\quad \rho > 0;\quad \phi > 0\} \tag{37}$$

The optimisation was performed using a constrained non-linear global optimisation procedure using a global hill-climbing algorithm (GLOBAL OPTIMIZATION 9, Loehle Enterprises, Naperville, IL, USA) within the MATHEMATICA® 9 environment (Wolfram Research Inc., Champaign, IL, USA).

Tables

Table 1. Maximum stress $\sigma_{\max}$, associated maximum strain $\varepsilon_{\max}$, and elastic modulus *E* of the fibrous scaffold in circumferential and longitudinal direction obtained from experimental tensile test data. Values are given as mean ± standard deviation.

Degradation time (days)	Circumferential direction			Longitudinal direction		
	$\sigma_{\max}$ (MPa)	$\varepsilon_{\max}$ (%)	*E* (MPa)	$\sigma_{\max}$ (MPa)	$\varepsilon_{\max}$ (%)	*E* (MPa)
0	1.02 ± 0.23	46 ± 11	5.33 ± 1.53	0.071 ± 0.016	69 ± 24	0.14 ± 0.09
4	0.81 ± 0.17	32 ± 3	5.57 ± 1.29	0.032 ± 0.005	38 ± 17	0.11 ± 0.03
7	0.69 ± 0.20	26 ± 4	5.31 ± 1.15	0.020 ± 0.007	19 ± 9	0.15 ± 0.08
11	0.51 ± 0.12	18 ± 2	4.77 ± 1.32	0.016 ± 0.004	16 ± 4	0.13 ± 0.06
14	0.43 ± 0.10	14 ± 2	4.83 ± 1.02	0.013 ± 0.003	18 ± 6	0.09 ± 0.05
17	0.37 ± 0.08	13 ± 4	4.08 ± 0.73	0.010 ± 0.006	13 ± 6	0.10 ± 0.08
21	0.35 ± 0.08	10 ± 1	5.00 ± 0.90	0.012 ± 0.004	18 ± 8	0.10 ± 0.07
24	0.32 ± 0.11	12 ± 3	3.85 ± 0.84	0.008 ± 0.002	13 ± 10	0.08 ± 0.04
28	0.38 ± 0.004	12 ± 2	4.81 ± 0.35	0.01 ± 0.007	8 ± 2	0.15 ± 0.02

Table 2. Constitutive parameters for fibrous scaffold at various degradation time points T. The parameters in bold characters are those that were allowed to vary during the final identification procedures for degradation times of 4 to 28 days.

T	0	4	7	11	14	17	21	24	28
$\rho = \xi_a/\xi_b$	**1.27013**	1.27013	1.27013	1.27013	1.27013	1.27013	1.27013	1.27013	1.27013
β	**899.505**	899.505	899.505	899.505	899.505	899.505	899.505	899.505	899.505
c_1	**34.8434**	**48.3711**	**49.6159**	**43.1166**	**46.5156**	**37.7936**	**47.0107**	**41.7615**	**51.0792**
c_2	**401.748**	**731.563**	**978.899**	**826.156**	**1196.26**	**898.147**	**1338.21**	**997.108**	**1806.08**
p	**0.443004**	0.443004	0.443004	0.443004	0.443004	0.443004	0.443004	0.443004	0.443004
ϕ	**0.999339**	**0.999614**	**0.999551**	**0.999579**	**0.999687**	**0.999577**	**0.999663**	**0.99976**	**0.999631**
Strain (%)	16	16	16	16	13	10	9	12.5	9
r^2 (X-fibre)	0.99941	0.998243	0.98587	0.966938	0.995167	0.992996	0.99742	0.871015	0.952633
r^2 (// fibres)	0.99988	0.999684	0.999757	0.999905	0.999666	0.999906	0.999765	0.999833	0.999765

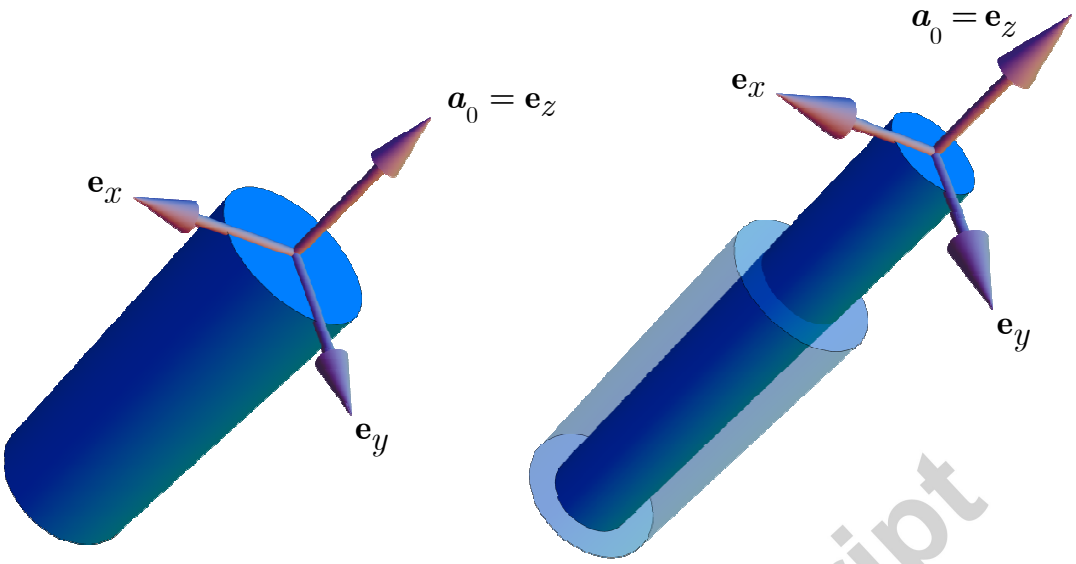

a/ b/

Figure 1. Illustration of the kinematics of a perfectly incompressible polymer rod subjected to uniform extension along its longitudinal axis, collinear with the unit vector $\mathbf{a_0}$: a/ undeformed configuration; b/deformed configuration.

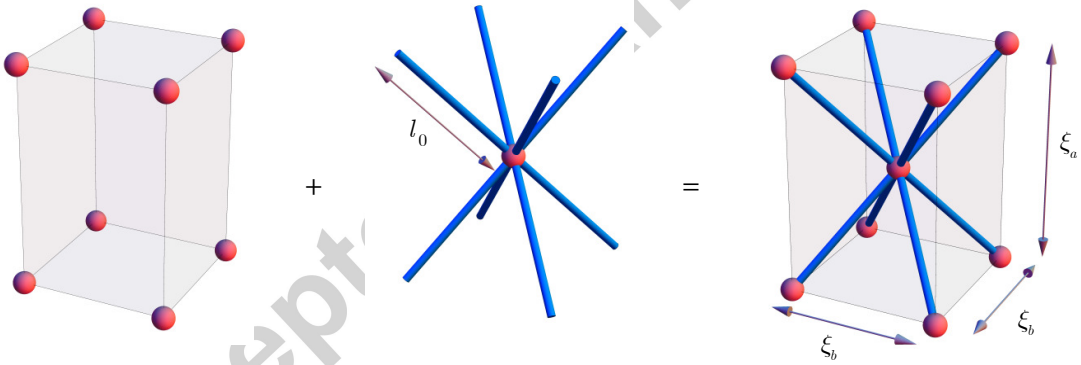

Associated parameters

c_1: controls the shear properties of the scaffold material.

β: controls the bulk properties of the scaffold material (compressibility).

Associated parameters

c_1: controls the shear properties of individual polymer fibres.

c_2: scales the shear properties of individual polymer fibres according to the strain along the fibre.

p: controls the shape of the stress-strain curve of the bulk material making up the polymer fibres and that of these fibres when contributing to the macroscopic properties of the scaffold material.

Associated parameters

$\rho = \xi_a/\xi_b$: controls the anisotropy of the unit cell and, ultimately, that of the macroscopic mechanics of the scaffold material.

ϕ: volume fraction of the polymer fibres with respect to the total volume of the scaffold material.

Figure 2. Schematic representation of the eight chain network model. The light grey solid volume represents the bulk material admitting the strain energy function ψ_{bulk} while the eight single polymer fibres represented as blue tubes are governed by the strain energy function ψ_{chain} (adapted from Kuhl et al. (2005)). In order to facilitate the physical interpretation and understanding of the constitutive model, the material parameters of the total strain energy function governing the elasticity of the scaffold material (Equation (16)) are explicitly described.

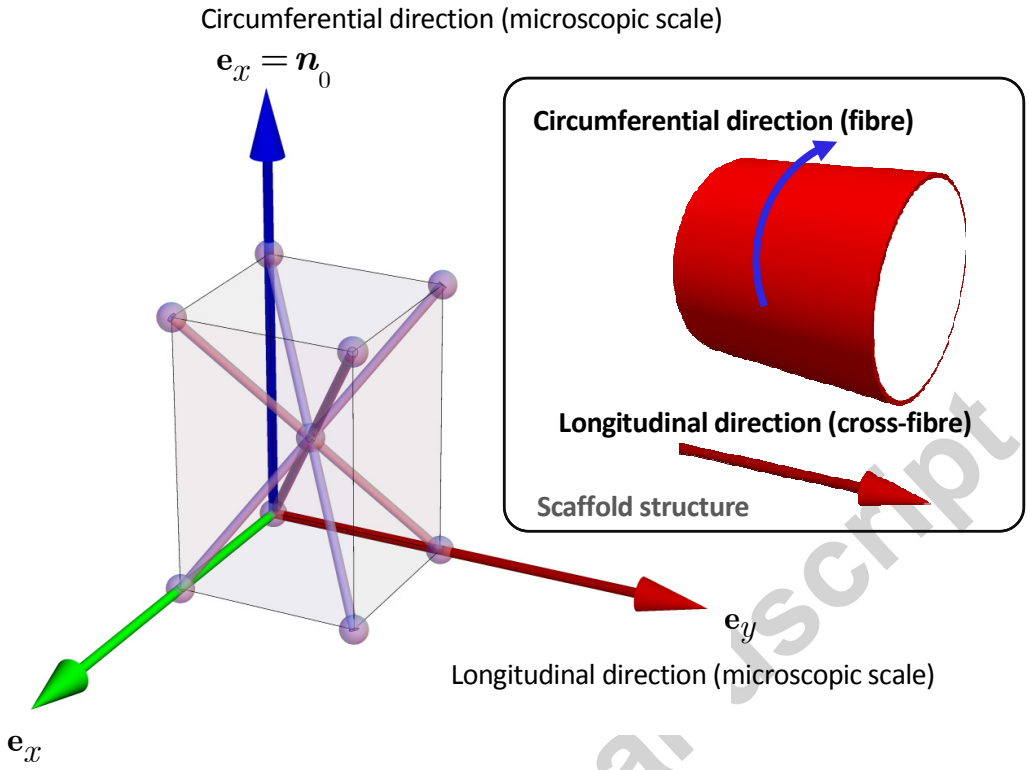

Figure 3. Orthonormal coordinate system describing the sample material directions with respect to the microscopic unit cell. The longitudinal direction ($z-axis$) of the electro-spun sample is assumed to be aligned with the vector $\mathbf{n}_0$ characterising the local direction from which transversely isotropy arises so that $\mathbf{e}_z = \mathbf{n}_0$. Inset: the electro-spun fibre scaffold is depicted in red. Macroscopic material directions (fibre and cross-fibre directions) are also indicated.

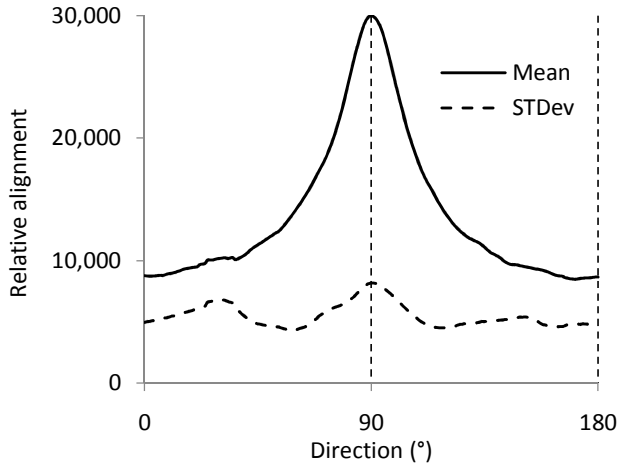

Figure 4. Normalised degree of fibre alignment of the electro-spun fibrous scaffold. The 90° direction indicates with the circumferential direction of the tubular scaffold, 0° and 180° coincide with the longitudinal scaffold direction.

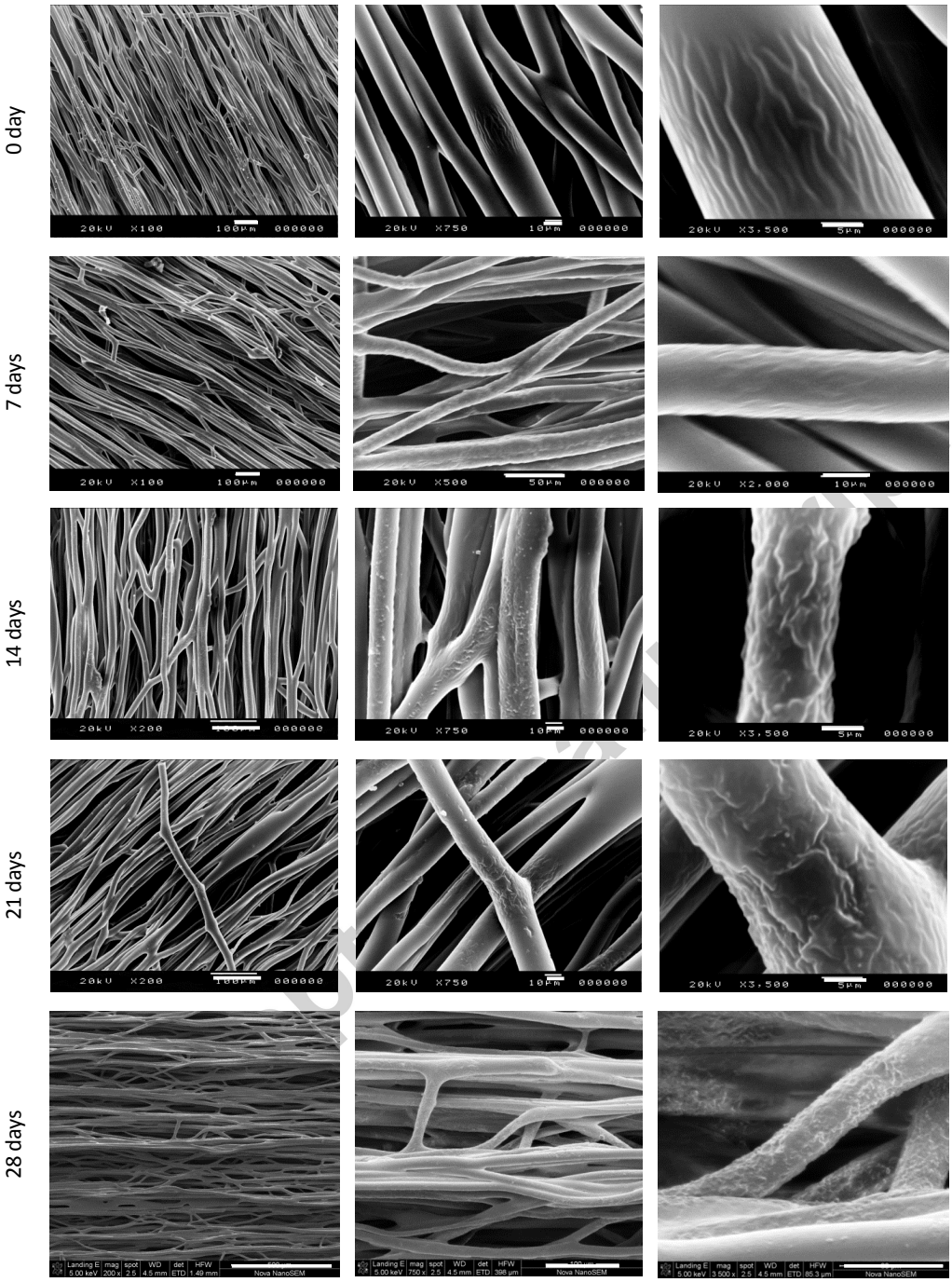

Figure 5. SEM micrographs illustrating the morphology of the electro-spun fibrous scaffold before and after degradation of 7, 14, 21 and 28 days. Magnification and length of the scale bar are provided for each micrograph per degradation time point from left to right: 0d: ×100, 100 µm; ×750, 10 µm; ×3500, 5 µm. 7d: ×100, 100 µm; ×500, 50 µm; ×2000, 10 µm. 14d: ×200, 100 µm; ×750, 10 µm; ×3500, 5 µm. 28d: ×200, 500 µm; ×750, 100 µm; ×3500, 30 µm

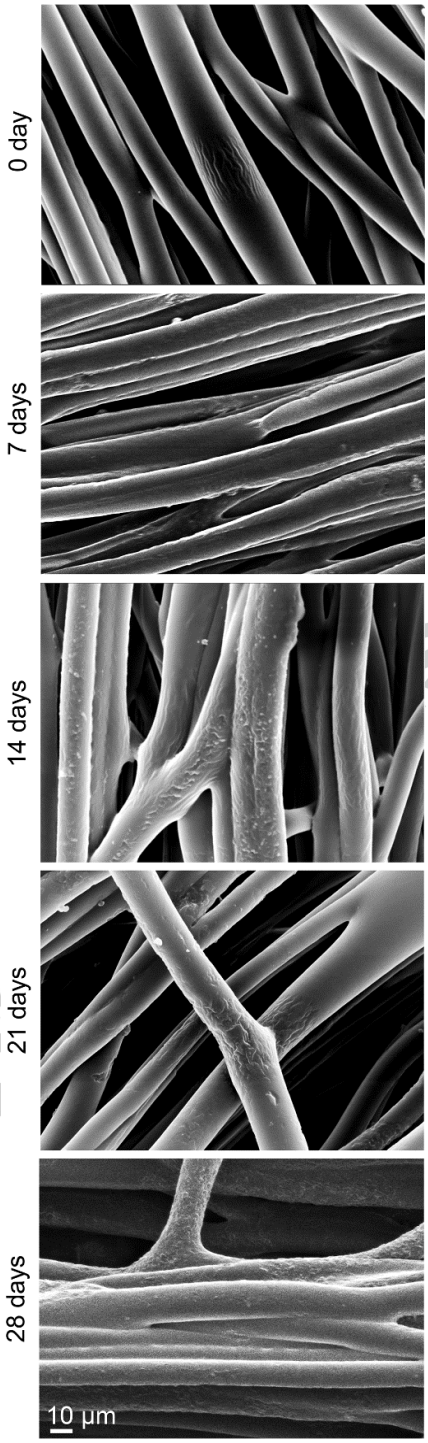

Figure 6. SEM micrographs of the same magnification showing scaffold fibres before and after degradation. The scale bar in the bottom image applies to all images.

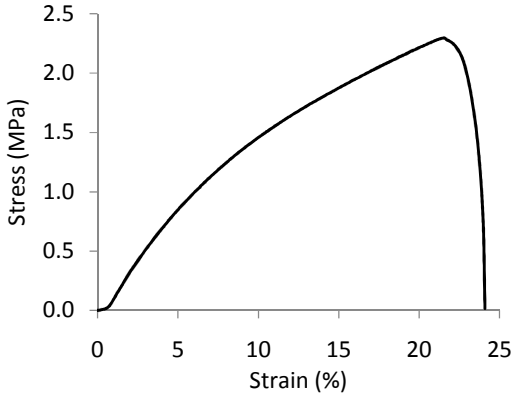

Figure 7. Stress versus strain data obtained from uniaxial tensile tests of bulk material.

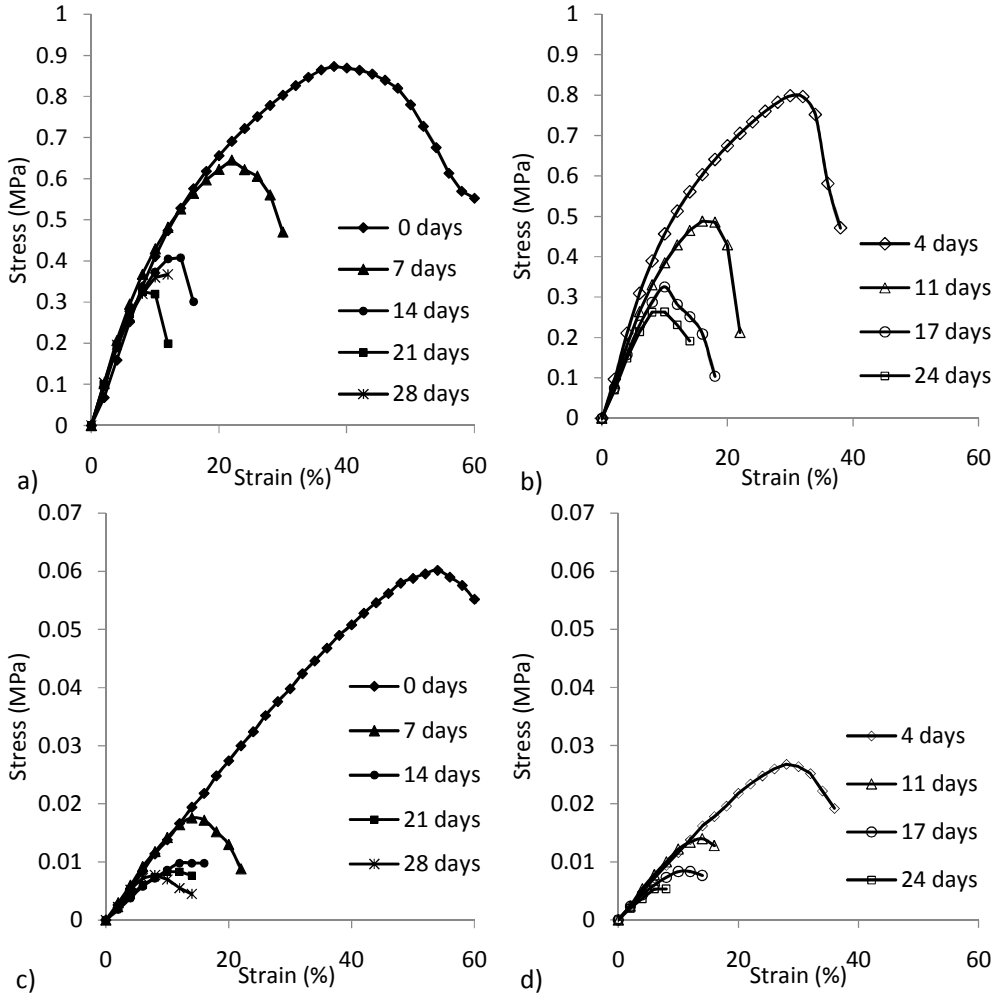

Figure 8. Averaged stress-strain curves of electro-spun scaffolds for tensile loading in circumferential direction (a, b) and longitudinal direction (c, d) for different degradation time points. (Data presented in tow time point groups for each direction to improve clarity.)

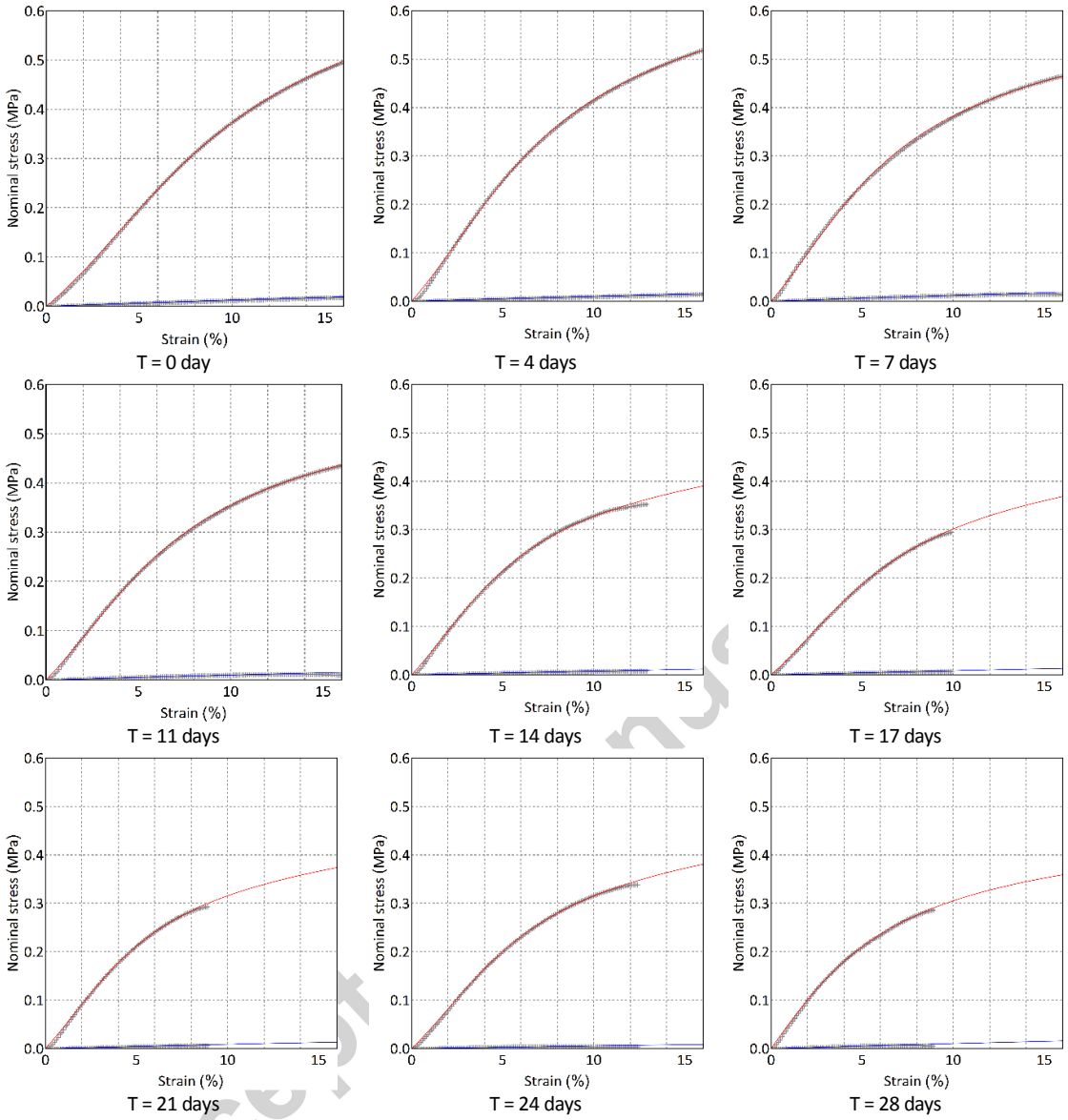

Figure 9. Theoretical (continuous line) and experimental strain-stress curves of the electro-spun scaffold for uniaxial extensions along the longitudinal and circumferential directions at various degradation times. Red: along the fibre direction; blue: orthogonal to the fibre direction.

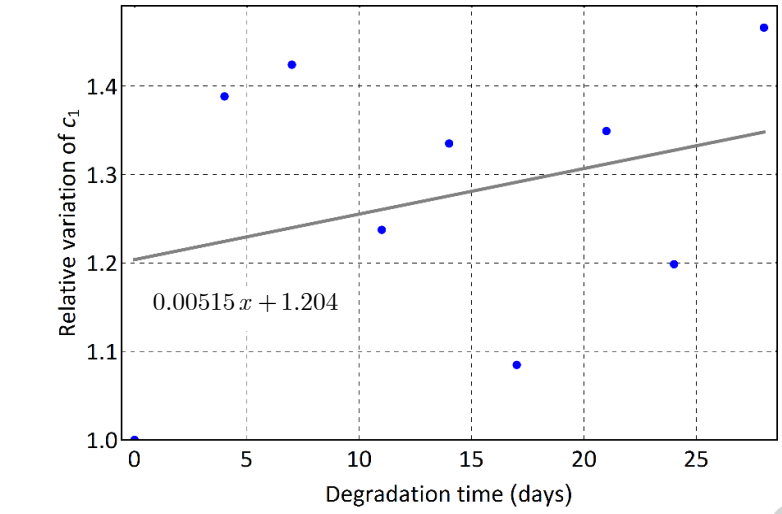

a)

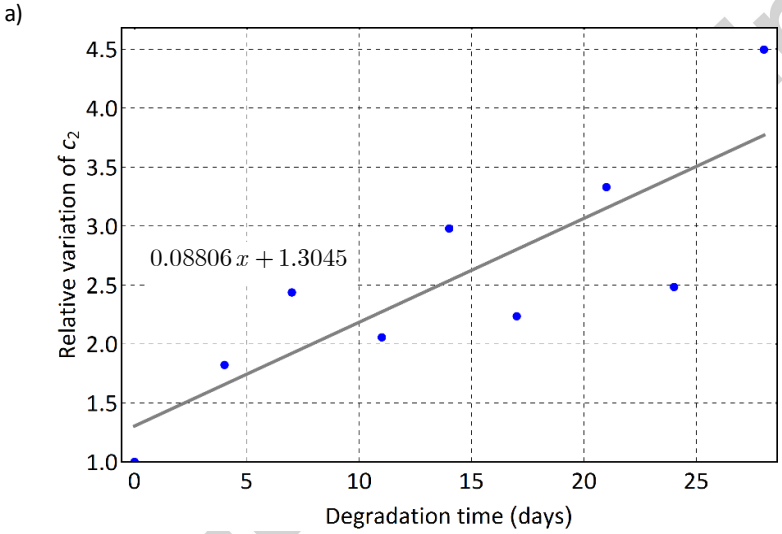

b)

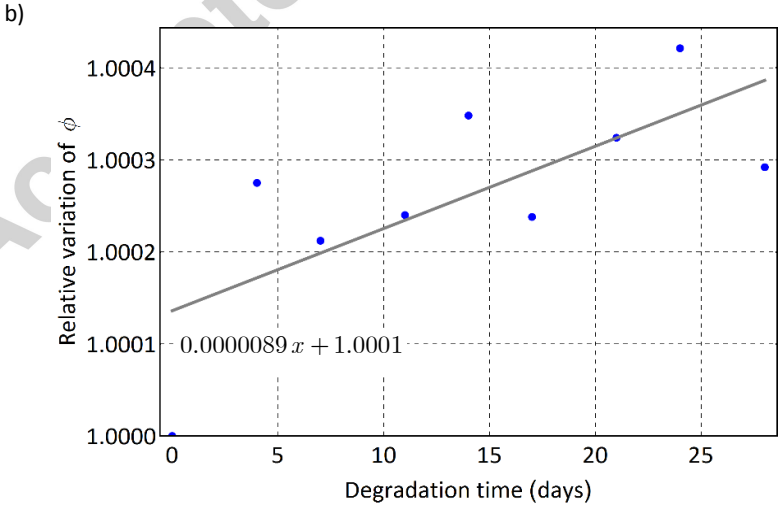

c)

Figure 10. Relative variations of the parameters of the constitutive model as a function of degradation time.